Department of Electrical and Computer Engineering

Modelling and Analysis of Semiconductor Optical Amplifiers for High-Speed Communication Systems Using Finite-Difference Beam Propagation Method

Suchi Barua

This thesis is presented for the Degree of
Master of Philosophy
of
Curtin University

December 2014

Declaration

To the best of my knowledge and belief, this thesis contains no material previously published by any other person except where due acknowledgement has been made.

This thesis contains no material which has been accepted for the award of any other degree in any university.

Signature: Suchi Barua

Date: 19/01/2015

Acknowledgement

First and foremost I thank God who gave me the grace and privilege to pursue my MPhil degree in Electrical and Computer Engineering, which turned out to be quite remarkable journey in spite of many challenges. Undertaking this MPhil has been a truly life-changing experience for me and it would not have been possible to do without the support and guidance that I received from my supervisors, colleagues, friends and many other people.

I would like to express my heartfelt gratitude to my supervisor Professor Sven Nordholm and co-supervisor Dr. Narottam Das who have been tremendous mentors for me to complete this task. A very big thank to you for your every bit of guidance, assistance, involvement and encouragement throughout the course duration to produce this thesis. I could not have asked for better role models, each inspirational, supportive, and patient. I could not be prouder of my academic roots and hope that I can in turn pass on the research values and the dreams that they have given to me. I am also thankful to Dr. Mohammed Razaghi, Assist Professor of University of Kurdistan, Iran for his continuous support and encouragement for the research works.

During this MPhil period, I met a lot of nice people who were always willing to help me and made me feel the group as a big family. I really do not know how to express my gratitude to my beloved colleagues but the best wishes to them will be always given from my side.

My deep gratitude also goes to Curtin University and Curtin University Postgraduate Student Association (CUPSA) for providing the research support and student travel grant to attend the International Conferences in Spain and Singapore.

A special thanks to my family members for their support. Words cannot express how grateful I am to my parents and my sisters for all of the sacrifices that you've made on my behalf. Your prayer for me was what sustained me thus far. I would like to express appreciation to my husband for his support during the course of this study which helped me making a successful completion of the degree. Finally, to my darling son Aarish for being such a good little baby that past ten months and making it possible for me to complete what I started.

Suchi Barua

Perth, Australia

December 2014

Abstract

The semiconductor optical amplifier (SOA) is used as an active nonlinear optical medium or device. It has many important features such as optical gain, operations with relatively low optical input power, small size, capability of large-scale integration and short response time. It has attracted lots of interests because of their application potential in the field of high-speed optical communications. It is visualized for all-optical signal processing tasks at very high bit rates that cannot be handled by electronics, such as wavelength conversion, signal regeneration, optical switching as well as logic gate operations.

In this work, we have used finite difference-beam propagation method (FD-BPM) to solve the nonlinear Schrödinger equation for different input pulse shape dependent propagation characteristics and gain saturation characteristics in SOAs. Using this useful method, we have considered various nonlinear effects in the SOA such as the self-phase modulation (SPM), two-photon absorption (TPA), group velocity dispersion (GVD), carrier depletion (CD), carrier heating (CH), spectral-hole burning (SHB) and gain spectrum dynamics in the model for analyzing the characteristics.

The theoretical investigation of ultrashort pulse propagation in SOA has fundamental importance for understanding of carrier dynamics and the nonlinear effects that determine pulse shaping. SOA's internal structures are related to different parameters. The output pulse can be changed due to the variation of input parameters, such as input pulse shape, input pulse width, input pulse energy. For this reason, in this project pulse shape dependent propagation characteristics depending on different parameters have been analyzed for the faster communication systems. In earlier report single pulse propagation has been performed in SOA for Secant hyperbolic and Gaussian pulse shape individually. But in our work we have considered Lorentzian pulse as well. We have investigated pulse propagation characteristics for these three pulse shapes depending on different parameters and

compared the results. The impact of variation of the SOA parameters on the saturation phenomena is also analyzed by numerical simulations. Higher output pulse energy was obtained by Gaussian pulse shape comparing with the Secant hyperbolic and Lorenztian pulse shapes. It is also found that, red shifting of output spectra is input pulse energy dependent but it does not depend on the CH relaxation time.

Moreover, the gain saturation characteristics in SOA has been analyzed and compared for different input pulse shapes. The saturated output pulse energy increases with the increase of pulsewidth for all the input pulse shapes. Secant hyperbolic pulse reaches to saturation faster compared to the Gaussian and Lorentzian pulses and it is true for all considered input pulsewidth and CH relaxation time. We have also investigated the autocorrelation traces for full width half maximum (FWHM). It shows how the output FWHM broadened in relation to the input FWHM depending on different input energies for different input pulse shapes. The output spectral shape broadens with the increase of input pulse energy and the input FWHM.

At this stage, there is no such technique is available to quantify the input pulse shape dependent propagation characteristics of high-speed devices for optical communication systems. For this reason, the input pulse shapes dependent pulse propagation characteristics and gain saturation characteristic in SOAs were studied in details and demonstrated the results in this thesis for future applications in high-speed communication systems.

Contents

List of Symbols

A		Coefficient of the stimulated emission
b_2	$cm^{-1}W^{-1}$	Instantaneous self phase modulation term due to Kerr effect
C	ms^{-1}	Velocity of light in vacuum
D	µm	Thickness of the active region
f_0	THz	Centre frequency of the pulse
$f_{(\tau)}$		Spectral hole burning function
g_0	cm^{-1}	Linear gain
$g(\tau,\omega)$	cm^{-1}	Gain spectrum of a semiconductor optical amplifier
$g_N(\tau)$	cm^{-1}	Saturated gain due to carrier depletion
h_1	$cm^{-1}\ pJ^{-1}$	The contribution of stimulated emission and free carrier absorption to the carrier heating gain reduction
h_2	$fs\ cm^{-1}\ pJ^{-2}$	The contribution of two-photon absorption
n		Number of sampling
n_2	$cm^2\ TW^{-1}$	Instantaneous nonlinear Kerr effect
$u(s)$		Unit step function
W	nm	Width of the active region
Z	µm	Propagation direction
v_g	ms^{-1}	Group velocity at the centre frequency of an optical pulse
A	$µm^2$	Effective area
A_1	$fs\ µm^{-1}$	Slope of the linear gain at ω_0
A_2	$fs^2\ µm^{-1}$	Curvature of the linear gain at ω_0
B_1	fs	Constant describing changes of slope (A_1) with saturation
B_2	fs^2	Constant describing changes of curvature (A_2) with saturation
L	µm	Length of SOA

P_{shb}	W	Spectral-hole burning saturation power
$V(\tau, z)$	$W^{1/2}$	Complex envelop function
W_s	pJ	Saturation energy
α_N		Linewidth enhancement factor due to the carrier depletion
α_T		Linewidth enhancement factor due to the carrier heating
β_2	$ps^2\,cm^{-1}$	Group velocity dispersion
γ	cm^{-1}	Linear loss
γ_{2p}	$cm^{-1}W^{-1}$	Two-photon absorption coefficient
τ	ps	Local time which propagates with the group velocity v_g at the center frequency of an optical pulse
τ_s	ps	Carrier lifetime
τ_{ch}	fs	Carrier heating relaxation time
τ_{shb}	fs	Spectral-hole burning relaxation time
ω_0	$rads^{-1}$	Center angular frequency of the pulse
$\Delta g_T(\tau)$	cm^{-1}	resulting gain change due to the CH and TPA
$\Delta\tau$	fs	Sampling time
Δz	μm	Propagation step
Γ		Confinement factor

List of Acronyms

BPM	Beam propagation method
CD	Carrier depletion
CH	Carrier heating
FD-BPM	Finite-difference BPM
FFT	First Fourier transformation
FFT-BPM	First Fourier transformation BPM
FWHM	Full width half maximum
GVD	Group velocity dispersion
MNLSE	Modified nonlinear Schrödinger equation
SHB	Spectral hole burning
SOA	Semiconductor optical amplifier
SPM	Self-phase modulation
TPA	Two photon absorption

List of Figures

List of Tables

LIST OF PUBLICATIONS

Referred Journal Papers

[1] S. Barua, N. Das, S. Nordholm, and M. Razaghi, “Analysis of nonlinear pulse propagation characteristics in semiconductor optical amplifier for different input pulse shapes”, International Journal of Electrical, Computer, Electronics and Communication Engineering, World Academy of Science, Engineering and Technology, Vol. 9, No. 1, pp. 16-20, January 2015.

[2] S. Barua, N. Das, S. Nordholm, and M. Razaghi, “Effect of input pulse shapes on semiconductor optical amplifiers gain saturation characteristics”, Submitted to the *Journal of Optical Engineering, SPIE*, USA.

[3] S. Barua, N. Das, S. Nordholm, and M. Razaghi, “Comparison of pulse propagation and gain saturation characteristics among different input pulse shapes in semiconductor optical amplifiers”, Submitted to the *Journal of Optics Communications, Elsevier Journal*, UK.

Referred Conference Papers

[1] S. Barua, N. Das, S. Nordholm, and M. Razaghi “Analysis of gain saturation characteristics in SOAs for different input pulse shapes” in proc. of the 14th International conference on Numerical Simulation of Optoelectronics devices (NUSOD 2014), pp. 77-78, Sep. 1-4, 2014. Palma de Mallorca, Spain.

Chapter 1
Introduction

The background of the research is briefly discussed in this chapter. The main objectives and the contribution of this thesis to future high-speed optical communications for next generation are discussed. It also contains the organization of the thesis chapters.

1.1 Background

Semiconductor optical amplifiers (SOAs) have become the key component in optical communication network for its application potentiality. The SOAs have attracted attention in optical amplification and optical switching at a very high-speed because of their small size, a low switching energy, non-linear characteristics, ability to integrate with other optical devices and moreover, simultaneous amplification and compression of the optical pulses. The SOA is an active non-linear optical medium which is showing great promise in high-speed optical switching, all-optical wavelength conversion, regeneration, wavelength selection, booster and in-line amplification, in-node optical pre-amplification, optical signal processing and routing [1-3].

In recent years, significant research effort has been focused on all optical functions and applications of non-linear waveguides such as SOAs and laser diodes. Therefore, characterization of the SOA operational functionalities and optimization of its performance for amplification and switching are essential and challenging features. The SOA is a non-linear device and its internal structure related to different parameters. The output pulse of the SOA can be changed due to the variation of input

parameters, such as input pulse shape, input pulse width and input pulse energy. For this reason, in this research, pulse shape dependent propagation characteristics that depend on different parameters have been analyzed in details for the faster communication systems. The purpose of SOA modeling is to relate the input variables such as input pulse shapes, input pulse energy levels, input pulsewidth of the amplifier with output variables, such as the output signal power, saturation output power, gain saturation etc.

1.2 Objectives

The main objective of this thesis is to analyze the input pulse shape dependent propagation characteristics and gain saturation characteristics in SOAs and related devices for faster communication systems. All optical functional devices should operate at faster rates with the increase of bit rates of optical fiber communications. For this reason, pulse propagation and gain characteristics have been investigated in details with different input pulse shapes depending on different parameters.

Due to the high demand of speed for the communications systems, such as computer communications, internet, data processing and mobile networks etc. we need high-speed communication devices for the faster communication systems. This new high-speed device will be useful for high-speed internet, data mining or fast train (e.g. mining side) communication systems. This research will contribute significantly to the high-speed communication systems for future or next generation's communications. The modeling results of this research will work of direct relevance to the users and manufacturers of semiconductor or communication devices. With a growing network, the results will be of extreme value to the Australian Telecommunication networks in their strategy to maintain the high-speed communications without interception or interruption. Finite-difference beam propagation method (FD-BPM) will be used to solve modified non-linear Schrödinger equation (MNLSE) to obtain the device parameters for designing the high-speed communication devices for a reliable high-communication system for the next generations [4-11].

1.3 Contribution of the Thesis

The research has mainly focused on modelling and simulation of pulse shape dependent propagation characteristics in SOAs for the design of high speed communication devices and systems. In earlier research, single pulse propagation had been performed in SOAs for Secant hyperbolic and Gaussian pulse shapes individually [8, 12-14]. In our research we have considered Lorentzian pulse in addition to Secant hyperbolic and Gaussian pulse. Pulse shape dependent propagation characteristics has not been analyzed and compared in SOAs yet. In this research, we have investigated pulse propagation characteristics for these three types of pulses depending on different input pulse energy levels, carrier heating (CH) relaxation time and compared these results.

In addition, the gain saturation characteristics in SOAs have been analyzed and compared for different input pulse shapes. Nowadays, the very high-speed optical transmission is a relevant problem in relation to the gain saturation in SOAs. Analysis of the gain in linear and non-linear regimes of SOA is very important for this reason. The gain saturation characteristics has been investigated and compared depending on different input parameters such as, pulse width and the CH relaxation time.

We have also investigated the autocorrelation traces for full width half maximum (FWHM). It shows how the output FWHM broadened in relation to the input FWHM depending on different input energies for different input pulse shapes.

At this stage, there is no such technique available to quantify the pulse shape dependent propagation characteristics of high-speed devices for communication systems. So the input pulse shapes dependent pulse propagation characteristics were studied, measured and demonstrated in this thesis.

1.4 Thesis Outline

This thesis contains six chapters and the organization is shown in figure 1. The thesis is organized as follows.

Chapter 1 covers the background of the research, objectives of the thesis and the contribution of the research.

Chapter 2 describes the SOA structure, SOA non-linearities and pulse propagation in SOA. It also covers the formulation of MNLSE and simulation method (FD-BPM) for short optical pulses in SOAs.

Chapter 3 explains the propagation characteristics of different input pulse shapes in SOA depending on different input parameters.

Chapter 4 contains the gain saturation characteristics of different input pulse shapes depending on different input parameters. Here, the gain saturation characteristics for three input pulse shapes have been analyzed and compared.

Chapter 5 explains the autocorrelation traces of FWHM. The normalized difference of FWHM has been calculated and compared for different input pulse shapes.

Chapter 7 concludes this thesis and some suggestions are given for future work.

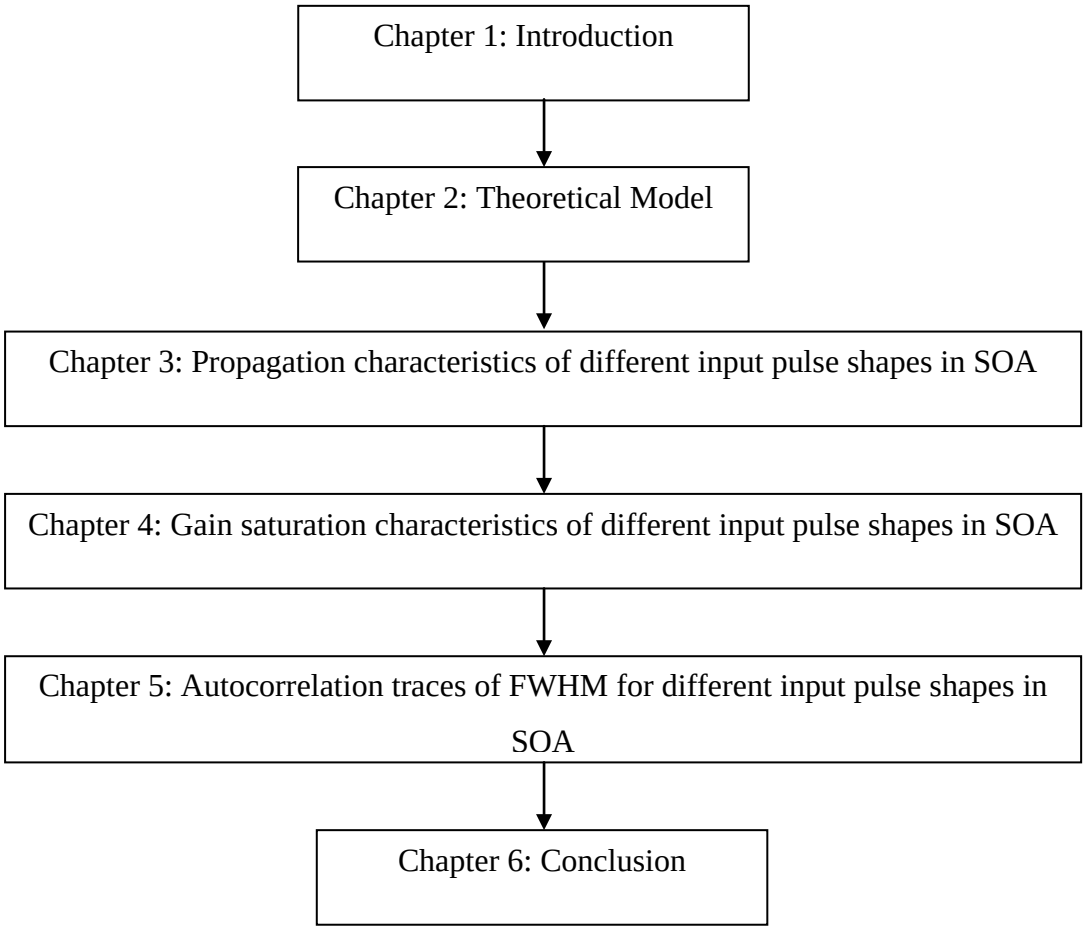

Figure 1: Organization of the chapters.

Chapter 2
Theoretical Model

This chapter contains about the SOA structure, non-linearities in SOAs, the MNLSE and FD-BPM which is used in the entire simulation of this research project.

2.1 SOA Structure

The SOA is an optoelectronic component composed of an optical waveguide. It is similar to a laser diode where the end mirrors are replaced with anti-reflection coatings. The SOA is coated with an input and output facets as shown in the schematic diagram in Figure 2.1. When an input optical signal injected into a SOA from the input facet side through the active region it will experience gain (amplification) under certain conditions. The gain is achieved by applying an external electrical current to the SOA [15].

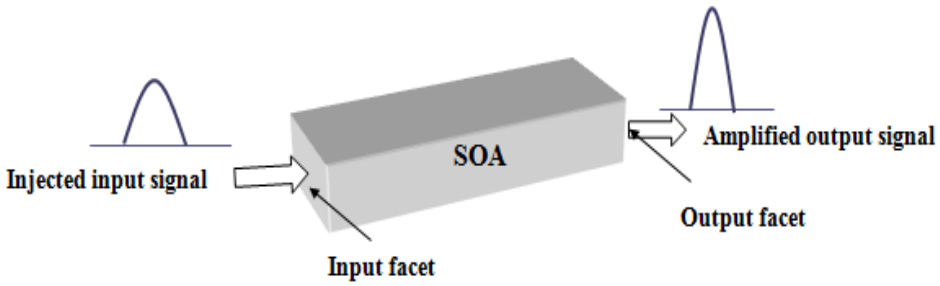

Figure 2. 1: Schematic diagram for pulse propagation in SOA.

2.2 Main Non-linearities in SOAs

The non-linear features in SOAs are important for wavelength conversion and switching which are widely used in high-speed photonic devices or networks. These

features are very useful where there is no conversion of optical signal to an electrical signal. The main non-linear effects involved in SOAs caused by the change of the carriers density induced by input signals. Those are self gain modulation (SGM), self-phase modulation (SPM), cross gain modulation (XGM), cross phase modulation (XPM) and self induced non-linear polarization rotation (SPR) [1, 16-17].

In the operational regime of SOA, there is a variation of total carrier density and carrier distributions. This variation causes intraband and interband transitions. The interband transition changes the carrier density but does not affect the carrier distribution. However, the intraband transitions, such as spectral hole burning (SHB), carrier depletion (CD), two photon absorption (TPA) and CH change the carrier distribution in the conduction band [16-17]. Figure 2.2 shows the time-development of the population density in the conduction band after excitation.

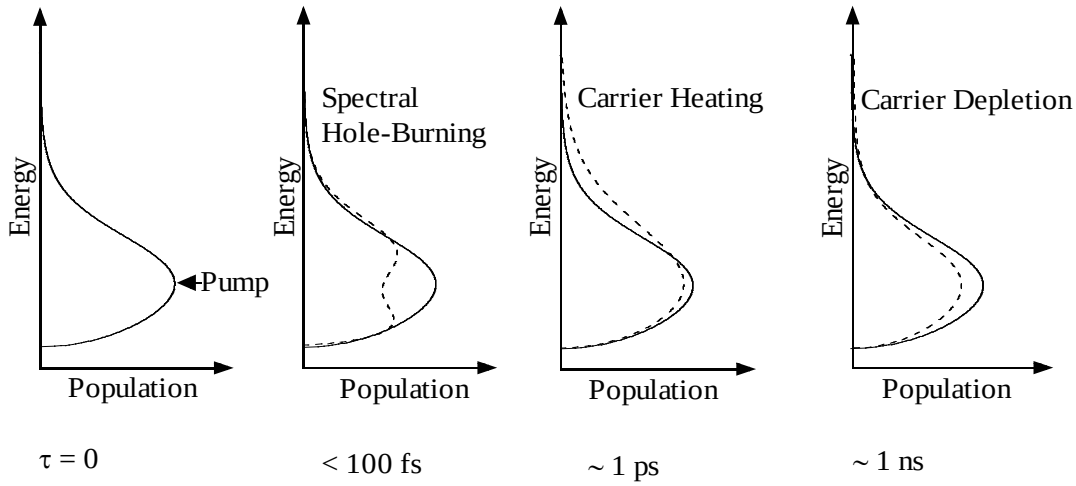

Figure 2. 2: Time development of population density in the conduction band after excitation in an SOA [4].

The arrow (pump) shown in Figure. 2.2 is the excitation energy. When a narrow-band strong pump beam excites the SOA, SHB occurs. SHB arises due to the finite value of intraband carrier-carrier scattering time (~ 50 – 100 fs), which sets the time scale on which a quasi-equilibrium Fermi distribution is established among the carriers in a band. Below 100 fs, the SHB effect is dominant. The SHB effect is relaxed approximately after 1 ps, and the CH effect becomes dominant. The process tends to increase the temperature of the carriers beyond the lattice's temperature. The main causes of heating the carriers are (1) the stimulated emission, since it involves

the removal of “cold” carriers close to the band edge, and (2) the free-carrier absorption, which transfers carriers to high energies within the bands. The “hot”-carriers relax to the lattice temperature through the emission of optical phonons with a relaxation time of ~ 0.5 – 1 ps. The effect of carrier depletion (CD) remains for about 1 ns. The stimulated electron-hole recombination depletes the carriers, thus reducing the optical gain. The band to band relaxation also causes carrier depletion, with a relaxation time ~ 0.2 – 1 ns. For ultra short optical pumping, the TPA effect also becomes important. An atom makes a transition from its ground state to the excited state by the simultaneous absorption of two laser photons. All these mechanisms (effects) are taken into account in the simulation and the formulation of MNLSE [4-5].

2.3 Derivation of Modified Non-linear Schrödinger Equation (MNLSE)

The theoretical model of short optical pulses propagation in SOAs is briefly discussed in this section. Starting from Maxwell’s equations, we reach to the propagation equation of short optical pulses in SOAs which are governed by the wave equation in the frequency domain [12, 18-20]:

$$\nabla^2 \bar{E}(x, y, z, \omega) + \frac{\varepsilon_r}{c^2} \omega^2 \bar{E}(x, y, z, \omega) = 0 \tag{2.1}$$

where, $\bar{E}(x, y, z, \omega)$ is the electromagnetic field of the pulse in the frequency domain, c is the velocity of light in vacuum and ε_r is the non-linear dielectric constant which is dependent on the electric field in a complex form. By using the slowly varying envelope approximation and integrating the transverse dimensions, the pulse propagation equation in SOAs is [12, 21]:

$$\frac{\partial V(\omega, z)}{\partial z} = -i \left\{ \frac{\omega}{c} \left[1 = \chi_m(\omega) + \Gamma \tilde{\chi}(\omega, N) \right]^{1/2} - \beta_0 \right\} V(\omega, z) \tag{2.2}$$

where, $V(\omega, z)$ is the Fourier-transform of $V(t, z)$ which represents pulse envelope, $\chi_m(\omega)$ is the background (mode and material) susceptibility, $\tilde{\chi}_m(\omega)$ is the complex susceptibility which represents the contribution of the active medium, N is the effective population density, β_0 is the propagation constant. The quantity Γ

represents the overlap/confinement factor of the transverse field distribution of the signal with the active region as defined in [12].

The MNLSE for the phenomenological model of semiconductor laser and amplifiers is obtained [22] by using mathematical manipulations [20-21], including the real part of the instantaneous non-linear Kerr effect as a single non-linear index n_2 and by adding the TPA term.

In this research, the following MNLSE [4-5, 8-11, 23-24] is used for the simulation of pulse propagation with different input pulse shapes in SOAs. This MNLSE is used the complex envelope $V(\tau, z)$ function of an optical pulse which is given as follows.

$$\left[\frac{\partial}{\partial z}-\frac{i}{2}\beta_2\frac{\partial^2}{\partial\tau^2}+\frac{\gamma}{2}+\left(\frac{\gamma_{2p}}{2}+ib_2\right)\left|V(\tau,z)\right|^2\right]V(\tau,z)=\left\{\frac{1}{2}g_N(\tau)\left[\frac{1}{f(\tau)}+i\alpha_N\right]+\right.$$

$$\left.\frac{1}{2}\Delta g_T(\tau)(1+i\alpha_T)-i\frac{1}{2}\frac{\partial g(\tau,\omega)}{\partial\omega}|_{\omega_0}\frac{\partial}{\partial\tau}-\frac{1}{4}\frac{\partial^2 g(\tau,\omega)}{\partial\omega^2}|_{\omega_0}\frac{\partial^2}{\partial\tau^2}\right\}V((\tau,z) \qquad (2.3)$$

Here,

$$g_N(\tau)=g_0\exp\left(-\frac{1}{W_s}\int_{-\infty}^{\tau}e^{-s/\tau_s}\left|V(s)\right|^2 ds\right) \qquad (2.4)$$

$$f(\tau)=1+\frac{1}{\tau_{shb}P_{shb}}\int_{-\infty}^{+\infty}u(s)e^{-s/\tau_{shb}}\left|V(\tau-s)\right|^2 ds \qquad (2.5)$$

$$\Delta g_T(\tau)=-h_1\int_{-\infty}^{+\infty}u(s)e^{-s/\tau_{ch}}(1-e^{-s/\tau_{shb}})\left|V(\tau-s)\right|^2 ds$$

$$-h_2\int_{-\infty}^{+\infty}u(s)e^{-s/\tau_{ch}}(1-e^{-s/\tau_{shb}})\left|V(\tau-s)\right|^4 ds \qquad (2.6)$$

$$\left.\frac{\partial g(\tau,\omega)}{\partial\omega}\right|_{\omega_0}=A_1+B_1\left[g_0-g(\tau,\omega_0)\right] \qquad (2.7)$$

$$\left.\frac{\partial^2 g(\tau,\omega)}{\partial\omega^2}\right|_{\omega_0}=A_2+B_2\left[g_0-g(\tau,\omega_0)\right] \qquad (2.8)$$

$$g(\tau,\omega_0)=g_N(\tau,\omega_0)/\,f(\tau)+\Delta g_T(\tau,\omega_0) \qquad (2.9)$$

Here, the frame of the local time $\tau\ (=t-z/v_g)$ propagates with the group velocity v_g at the centre frequency of an optical pulse. The slowly varying envelope approximation is used in (2.3), where the temporal variation change of the complex

envelope function is very slow compared with the cycle of an optical field. In (2.3), $V(\tau, z)$ is the time domain complex envelope function of an optical pulse and $|V(\tau, z)|^2$ corresponds to the optical power, and β_2 is the GVD. γ is the linear loss, γ_{2p} is the TPA coefficient, $b_2 (= \omega_0 n_2 / cA)$ is the instantaneous SPM term due to the instantaneous non-linear refractive index n_2 (Kerr effect), $\omega_0 (= 2\pi f_0)$ is the centre angular frequency of the pulse, $A (= wd / \Gamma)$ is the effective area (d and w are the thickness and width of the active region, respectively, and Γ is the confinement factor). $g_N(\tau)$ is the saturated gain due to CD, g_0 is the linear gain, W_s is the saturation energy, τ_s is the carrier lifetime, $f(\tau)$ is the SHB function, P_{shb} is the SHB saturation power, τ_{shb} is the SHB relaxation time, and α_N and α_T are the line width enhancement factor associated with the gain changes due to the CD and CH. $\Delta g_T(\tau)$ is the resulting gain change due to the CH and TPA, $u(s)$ is the unit step function, τ_{ch} the CH relaxation time, h_1 is the contribution of stimulated emission and free-carrier absorption to the CH gain reduction, and h_2 is the contribution of TPA. Finally, A_1 and A_2 are the slope and the curvature of the linear gain at ω_0 respectively, while B_1 and B_2 are constants describing changes in these quantities with saturation. In this simulation, the gain spectrum of an SOA is approximated by the following second-order Taylor expansion in $\Delta\omega$:

$$g(\tau, \omega) = g(\tau, \omega_0) + \Delta\omega \left.\frac{\partial g(\tau, \omega)}{\partial \omega}\right|_{\omega_0} + \frac{(\Delta\omega)^2}{2} \left.\frac{\partial^2 g(\tau, \omega)}{\partial \omega^2}\right|_{\omega_0} \tag{2.10}$$

The coefficients $\partial g(\tau, \omega)/\partial\omega|_{\omega_0}$ and $\partial^2 g(\tau, \omega)/\partial\omega^2|_{\omega_0}$ are related to A_1, A_2, B_1 and B_2 as given by (2.7) and (2.8). The same values of A_1, A_2, B_1 and B_2 as for an AlGaAs/GaAs bulk SOA are assumed. Figure 2.3 shows the gain spectra given by a second-order Taylor expansion about the pulse centre frequency with derivatives of $g(\tau, \omega)$ by (2.7) and (2.8). The solid line shows the unsaturated gain spectrum having $g_0 (= g(\tau, \omega_0))$ of 92 cm^{-1} at ω_0. The dotted line is a saturated gain spectrum having $g_0 / 2$ (= 46 cm^{-1}) at ω_0, and the dashed-dotted line is a strongly saturated gain spectrum having $g(\tau, \omega_0)$ of 0 cm^{-1} at ω_0. The pump frequency ω_0 is set to near the

gain peak, and the linear gain is 92 cm^{-1} at ω_0. The gain bandwidth is about the same as the measured value for an AlGaAs/GaAs bulk SOA [25]. A much wider gain bandwidth can be expected for an InGaAsP/InP bulk SOA [26]. With a decrease in the carrier density, the gain decreases and the peak position is shifted to a lower frequency because of the band-filling effect.

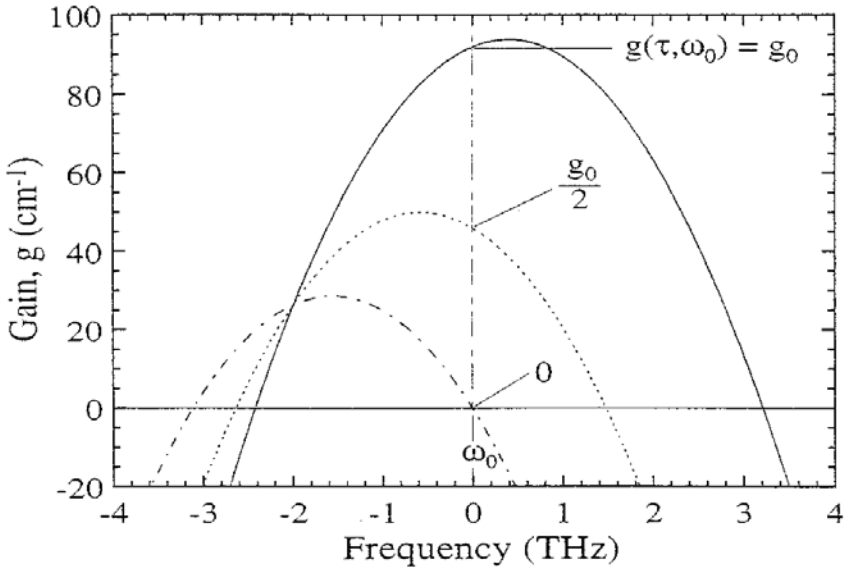

Figure 2. 3: Gain spectra given by the second-order Taylor expansion [4, 7-8].

This MNLSE was initially used for the analysis of 'solitary pulse' propagation in an SOA [22]. Later, a complex envelope function V (τ, 0) at the input side of the SOA has been introduced for the simulation of pulse propagation in an SOA using the FD-BPM [4-5, 8-11, 13, 24]. The MNLSE has been used in this research in conjunction with the FD-BPM for investigating pulse propagation characteristics, gain saturation characteristics and autocorrelation traces for the output FWHM.

2.4 Finite-Difference Beam Propagation Method (FD-BPM)

All the derivative terms appearing in the MNLSE, as well as in the boundary conditions, are replaced by the central differences approximation to solve a boundary value problem by the finite-differences method. Here, the central differences are used

because of greater accuracy [7]. The finite-differences (central differences) are applied to solve the MNLSE for this research work.

Generally, the fast Fourier transformation BPM (FFT-BPM) [27-28] is used for analysis of the optical pulse propagation in optical fibers by successive iterations of the Fourier transformation and the inverse Fourier transformation. In the FFT-BPM, the linear propagation term (GVD term) and phase compensation terms (other than GVD, first- and second- order gain spectrum terms) are separated in the non-linear Schrödinger equation for the individual consideration of the time and frequency domain for the optical pulse propagation. However, in this model, equation (2.3) includes the dynamic gain change terms, i.e., the first- and second- order gain spectrum terms which are the last two terms of the right side of equation (2.3). Therefore, it is not possible to separate equation (2.3) into the linear propagation term and phase compensation term, and it is difficult to calculate equation (2.3) using the FFT-BPM. For this reason, FD-BPM [6, 7] is used to solve this MNLSE. After replacing the time derivative terms of equation (2.3) by the central-difference approximation equation (2.11) and integrate equation (2.3) with the small propagation step Δz, the tridiagonal simultaneous matrix equation (2.12) is obtained [4, 8].

$$\frac{\partial}{\partial \tau} V_k = \frac{V_{k+1} - V_{k-1}}{2\Delta\tau}, \quad \frac{\partial^2}{\partial \tau^2} V_k = \frac{V_{k+1} - 2V_k + V_{k-1}}{\Delta\tau^2} \tag{2.11}$$

where, $V_k = V(\tau_k), V_{k+1} = V(\tau_k + \Delta\tau), V_{k-1} = V(\tau_k - \Delta\tau)$

$$-a_k(z+\Delta z)V_{k-1}(z+\Delta z) + \{1 - b_k(z+\Delta z)\} \times V_k(z+\Delta z) - c_k(z+\Delta z)V_{k+1}(z+\Delta z)$$
$$= a_k(z)V_{k-1}(z) + \{1 + b_k(z)\}V_k(z) + c_k(z)V_{k+1}(z) \tag{2.12}$$

where, k=1,2,3,.....,*n* and

$$a_k(z) = \frac{\Delta z}{2}\left[\frac{i\beta_2}{2\Delta\tau^2} + i\frac{1}{4\Delta\tau}\frac{\partial g(\tau,\omega.z)}{\partial\omega}\bigg|_{\omega_0,\tau_k} - \frac{1}{4\Delta\tau^2}\frac{\partial^2 g(\tau,\omega.z)}{\partial\omega^2}\bigg|_{\omega_0,\tau_k}\right] \tag{2.13}$$

$$b_k(z) = -\frac{\Delta z}{2}\left[\frac{i\beta_2}{\Delta\tau^2} + \frac{\gamma}{2} + \left(\frac{\gamma_{2p}}{2} + ib_2\right)|V_k(z)|^2 - \frac{1}{2}g_N(\tau_k,\omega_0,z)(1+i\alpha_N)\right.$$
$$\left. - \frac{1}{2}\Delta g_T(\tau_k,\omega_0,z)(1+i\alpha_T) - \frac{1}{2\Delta\tau^2}\frac{\partial^2 g(\tau,\omega.z)}{\partial\omega^2}\bigg|_{\omega_0,\tau_k}\right] \tag{2.14}$$

$$c_k(z) = \frac{\Delta z}{2}\left[\frac{i\beta_2}{2\Delta\tau^2} + i\frac{1}{4\Delta\tau}\frac{\partial g(\tau,\omega.z)}{\partial\omega}\bigg|_{\omega_0,\tau_k} - \frac{1}{4\Delta\tau^2}\frac{\partial^2 g(\tau,\omega.z)}{\partial\omega^2}\bigg|_{\omega_0,\tau_k}\right] \tag{2.15}$$

where, $\Delta\tau$ is the sampling time n is the number of sampling. If we know $V_k(z)$, (k = 1, 2, 3,.....n) at position z, we can calculate $V_k(z+\Delta z)$ at position of $z+\Delta z$ which is propagation of a step Δz from position z by using equation (2.12). It is not possible to directly calculate equation (2.12) because it is necessary to calculate the left-side terms $a_k(z+\Delta z)$, $b_k(z+\Delta z)$ and $c_k(z+\Delta z)$ of (2.12) from the unknown $V_k(z+\Delta z)$. Therefore, $a_k(z+\Delta z) \equiv a_k(z)$, $b_k(z+\Delta z) \equiv b_k(z)$ and $c_k(z+\Delta z) \equiv c_k(z)$ are defined and $V_k^{(0)}(z+\Delta z)$ as the zeroeth order approximation of $V_k(z+\Delta z)$ is obtained by using equation (2.12). Then, after substituting $V_k^{(0)}(z+\Delta z)$ in (2.12), $V_k^{(1)}(z+\Delta z)$ is obtained as the first-order approximation of $V_k(z+\Delta z)$. Finally accurate simulation results by iteration is obtained as used in [27] and [28].

Figure 2.4 shows the schematic diagram of the FD-BPM in time domain scale. Here, $\tau\ (=t-z/v_g)$ is the local time, which propagates with the group velocity v_g at the center frequency of an optical pulse and $\Delta\tau$ is the sampling time. z is the propagation direction and Δz is the propagation step. With this procedure, up to 3rd iteration is used for more accuracy of the simulations.

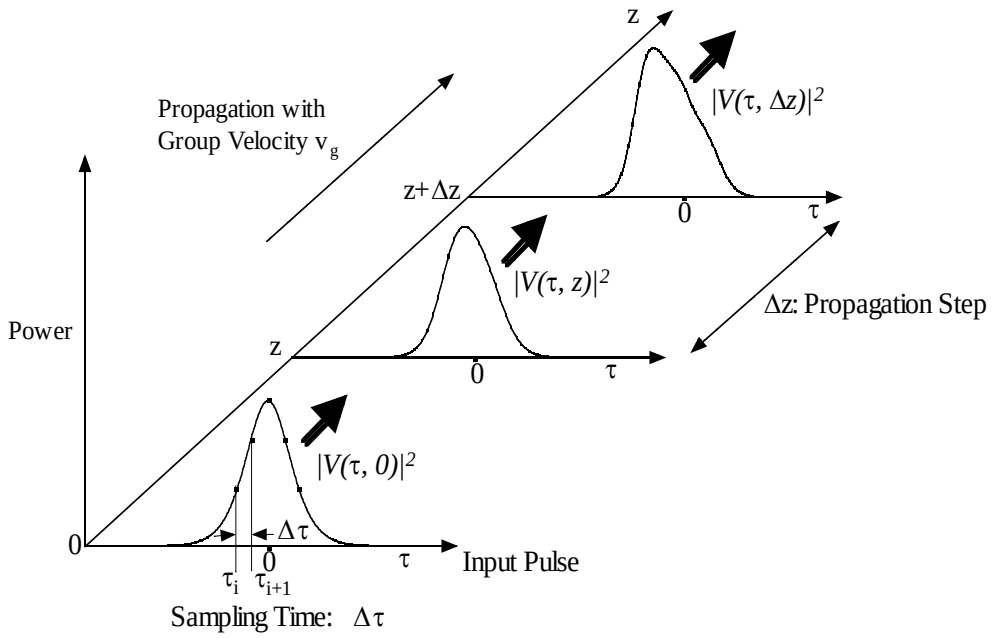

Figure 2. 4: Schematic diagram of FD-BPM for the simulation in time domain [4].

The FD-BPM is used for the simulation of several important characteristics in SOAs and optical fibers, namely, (1) single pulse propagation in SOAs [9, 24, 29-30], (2) two input pulses propagation in SOAs [8, 31] such as four wave mixing (FWM), (3) multiplexing of several input pulses using FWM [13], (4) optical phase-conjugation in SOAs using FWM [32] and (5) time-delay characteristics between pump-probe pulses of FWM in SOAs [4].

2.5 Nonlinear Pulse Propagation in SOA

All optical signal processing technique are playing a prominent role in high-speed communication systems to avoid electro-optic conversions that may create data-flow bottlenecks. Optical pulse propagation in SOAs has drawn wide attention due to a variety of all-optical functions such as wavelength conversion, signal regeneration, pulse reshaping and power limiting.

Figure 2.5 illustrates a simple simulation model for the propagation of optical pulses in an SOA. An optical pulse is injected into the input facet of the SOA, where the input pulse position is at $z = 0$. The pulse propagated over the length 500 μm of the SOA. Here, τ is the local time, $|V(\tau,0)|^2$ is the intensity (power) of input pulse (z = 0) and $|V(\tau,z)|^2$ is the intensity (power) of the output pulse after propagating a distance z (=500-μm) at the output side of SOA [4-5].

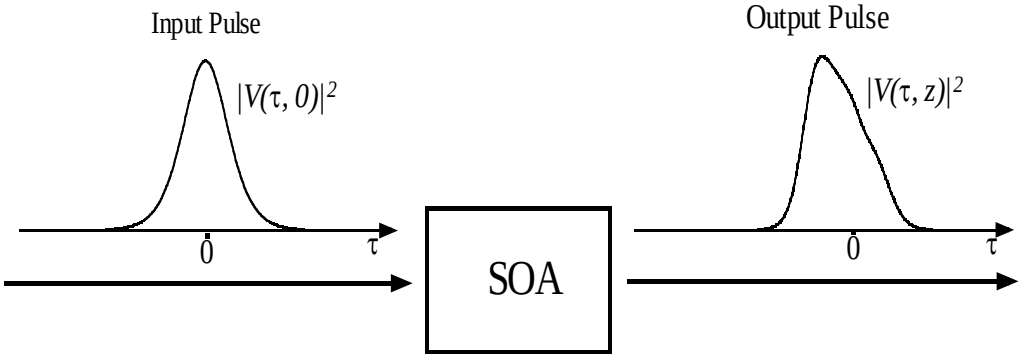

Figure. 2.5: Schematic diagram for the simulation of non-linear propagation pulses in SOA. Here, $|V(\tau,0)|^2$ and $|V(\tau,z)|^2$ are the input and output (after propagating a distance z) pulses power or intensity of the SOA [4-5].

2.6 Conclusion

This chapter describes the literature review and theoretical model which has been used for this research. It contains a brief overview on SOA structure, pulse propagation in SOA and SOA non-linearities. The derivation of MNLSE is explained and the MNLSE is used in this research for the simulation of pulse propagation that includes the SOA non-linearities. FD-BPM is considered as the best method for simulation of pulse propagation with small propagation steps. For this reason, FD-BPM is used to solve the MNLSE due to its short convergence time and excellent accuracy of simulation results.

Chapter 3
Input Pulse Shape Dependent Propagation Characteristics in SOA

In this chapter, the pulse dependent propagation characteristics of non-linear single optical pulse in bulk SOA (AlGaAs/GaAs, double heterostructure) have been analyzed and compared by using FD-BPM depending on input energy and CH relaxation time. The propagation characteristics have been investigated for three different input pulse shapes and the simulation results has been compared.

3.1 Introduction

Optical pulse propagation in SOAs has attracted much more attention due to its potential applications in high-speed optical communication systems, such as wavelength converter and switching. There are some applications in all optical signal processing such as clock recovery and optical time division demultiplexing, where the SOAs are used to amplify high energy optical pulses with pulse width of the order of picoseconds [31]. The propagation of picosecond optical pulses in SOAs is investigated numerically by taking into account CH, SHB and TPA effects as well as the non-linear refraction.

Secant hyperbolic and Gaussian pulses have been used for pulse propagation in previous works [8, 12-14]. In this research Lorentzian pulse also has been considered in addition to Secant hyperbolic and Gaussian pulse because pulse propagation in SOA is strongly dependent on the input pulse shapes. Understanding pulse amplification of different input pulse shapes in SOAs is important for optimizing the performance of SOA based optical regenerators and wavelength converters. The temporal and spectral characteristics have been analyzed and compared of these three input pulse shapes depending on input energy levels and CH relaxation time. The

FD-BPM has been used to solve the MNLSE which includes the carrier lifetime [6-7, 22] and the input pulse duration is much less than the carrier lifetime [12, 33-34].

Table 3.1: List of parameters used in simulation [9, 11]

Parameters Name	**Symbols**	**Values**	**Units**
Length of SOA	L	500	μm
Effective area	A	5	μm^2
Centre frequency of the pulse	f_0	349	THz
Linear gain	g_0	92	cm^{-1}
Group velocity dispersion	β_2	0.05	$ps^2\ cm^{-1}$
Saturation energy	W_s	80	pJ
Linewidth enhancement factor due to the carrier depletion	α_N	3.1	
Linewidth enhancement factor due to the CH	α_T	2.0	
The contribution of stimulated emission and free carrier absorption to the CH gain reduction	h_1	0.13	$cm^{-1}\ pJ^{-1}$
The contribution of two-photon absorption	h_2	126	$fscm^{-1}\ pJ^{-2}$
Carrier lifetime	τ_s	200	ps
CH relaxation time	τ_{ch}	700	fs
SHB relaxation time	τ_{shb}	60	fs
SHB saturation power	P_{shb}	28.3	W
Linear loss	γ	11.5	cm^{-1}
Instantaneous non-linear Kerr effect	n_2	-0.70	$cm^2\ TW^{-1}$
Two-photon absorption coefficient	γ_{2p}	1.1	$cm^{-1}W^{-1}$
Parameter describing second-order Taylor expansion of the dynamically gain spectrum.	A_1	0.15	$fs\ \mu m^{-1}$
	B_1	-80	fs
	A_2	60	$fs^2\ \mu m^{-1}$
	B_2	0	fs^2

In this simulation, the bulk SOA (AlGaAs/GaAs, double heterostructure) parameters are used as listed in Table 3.1 [9, 11]. The SOA length and wavelength are considered as 500 μm and 0.86 μm respectively. The simulation results are obtained with a propagation step Δz of 10 μm.

3.2 Mathematical formulations of different input pulse shapes

For the simulation of nonlinear pulse propagation and gain saturation characteristics in SOAs, following input pulse shapes are taken into consideration:

(i) Secant hyperbolic pulse

(ii) Gaussian pulse and

(iii) Lorentzian pulse

The mathematical representation of input pulse shapes in time domain is as follows:

(i) Secant hyperbolic pulse shape:

$$P(t) = \sqrt{\left(E_{in} / 2t_0\right)}\,\mathrm{sech}\left(t / t_0\right)$$

(ii) Gaussian pulse shape:

$$P(t) = \sqrt{\left(E_{in} / t_0\sqrt{\pi}\right)}\exp\left(-t^2 / 2{t_0}^2\right)$$

(iii) Lorentzian pulse shape:

$$P(t) = \sqrt{\left(2E_{in} / t_0\pi\right)}\left(1 + t^2 / {t_0}^2\right)^{-1}$$

here,

E_{in} = Input pulse energy in pJ

t = time in s

t_0 = parameter that controls the width of pulse in s

3.2.1 FWHM (t_p) calculation for different types of pulse shapes:

Table 3.2 shows the calculation of FWHM for the considered input pulse shapes:

Table 3.2 FWHM calculation for different types of pulse shapes

i) Secant hyperbolic pulse shape	$t_p = 2 \cosh^{-1}(\sqrt{2})\, t_0 = 1.7627\, t_0$
ii) Gaussian pulse shape	$t_p = 2\sqrt{\ln 2}\, t_0 = 1.665\, t_0$
iii) Lorentzian pulse shape	$t_p = 2\sqrt{(\sqrt{2}-1)}\, t_0 = 1.287\, t_0$

3.3 Simulation Results and Discussions

The simulation results of nonlinear optical pulse propagation characteristics in an SOA are discussed in this section. At first, the temporal and spectral characteristics of different input pulse will be discussed when the input pulse energy is 2 pJ, input pulse width is 10 ps, carrier lifetime is 200 ps and sampling time step (Δt) is 0.025 ps.

3.3.1 Pulse propagation characteristics for different input pulse shapes depending on input energy

3.3.1.1 Output waveform for different input pulse shapes

Figure 3.1 shows the input and output waveforms for (a) Secant hyperbolic pulse shape, (b) Gaussian pulse shape, and (c) Lorentzian pulse shape. For each pulse shape, a high output power (energy) has been observed due to the amplification or gain of the SOA. It is clearly observed that higher output pulse energy is achieved by Gaussian pulse comparing to other two pulse shapes. The calculated peak output powers are 4.2693 W, 4.5268 W, and 4.0091 W for Secant hyperbolic, Gaussian and Lorentzian pulses, respectively. When the input pulse energy increases, the output pulse energy also increases until gain saturation is reached. As the input pulse width is much shorter than the considered carrier lifetime, the leading edge of the pulse saturates the amplifier and the trailing edge experiences a lower gain, so the output pulse shape becomes asymmetric.

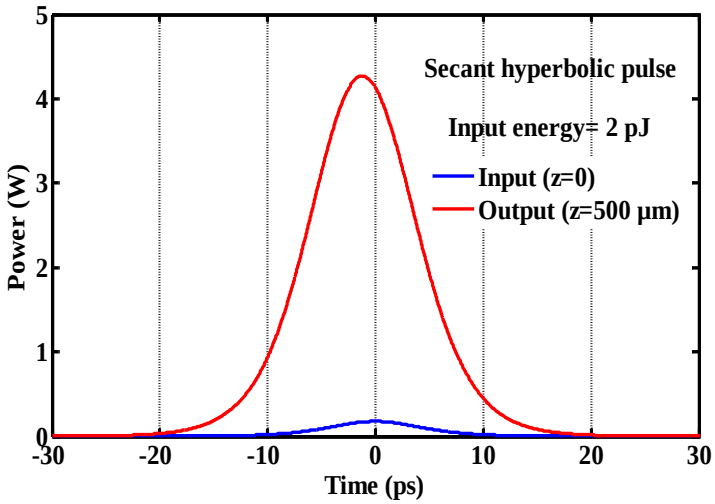

(a)

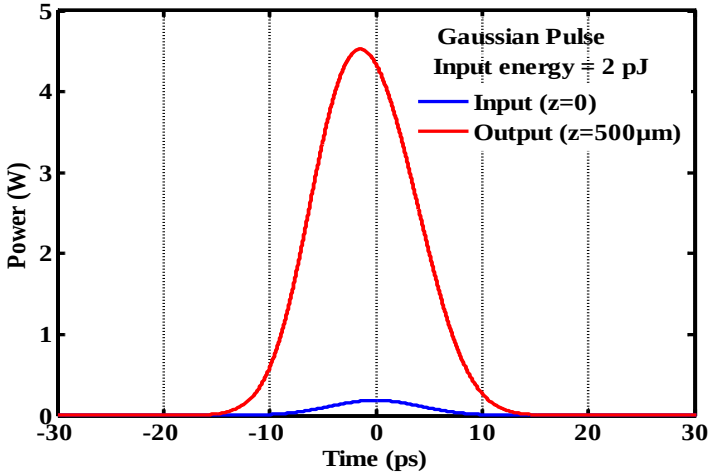

(b)

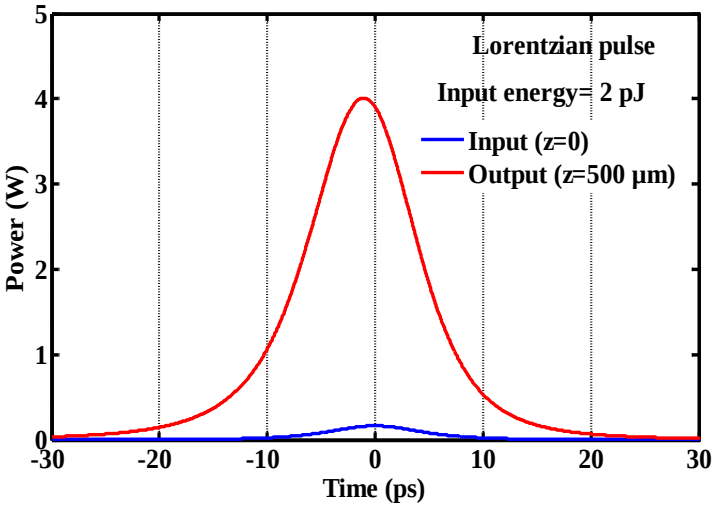

(c)

Figure 3.1: Waveform of input and output pulse shapes for (a) Secant hyperbolic, (b) Gaussian and (c) Lorentzian pulses.

3.3.1.2 Output spectra for different input pulse shapes

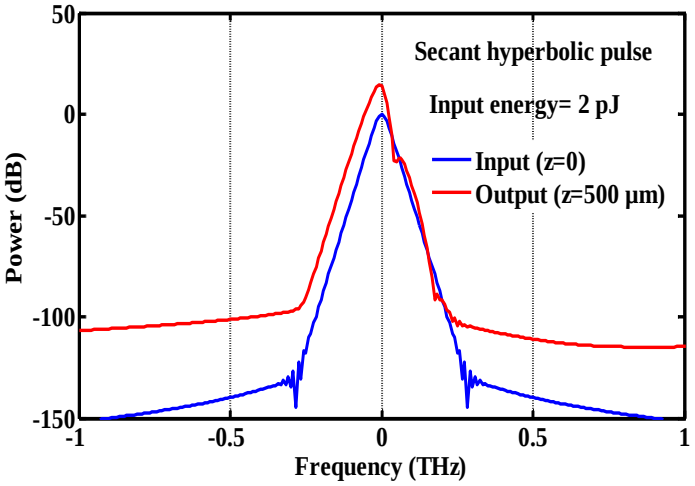

(a)

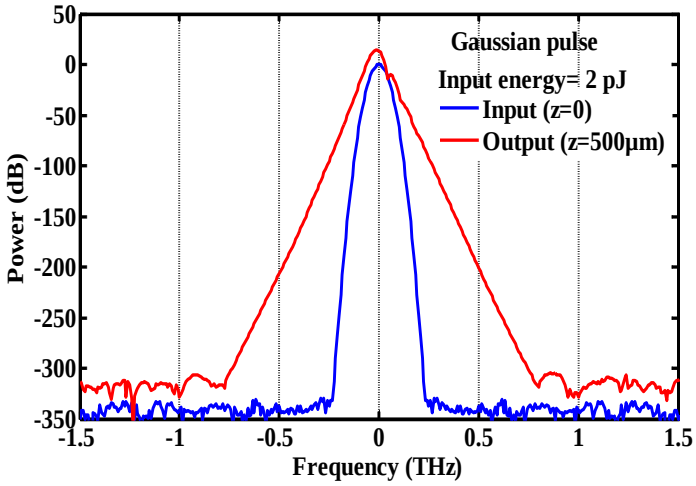

(b)

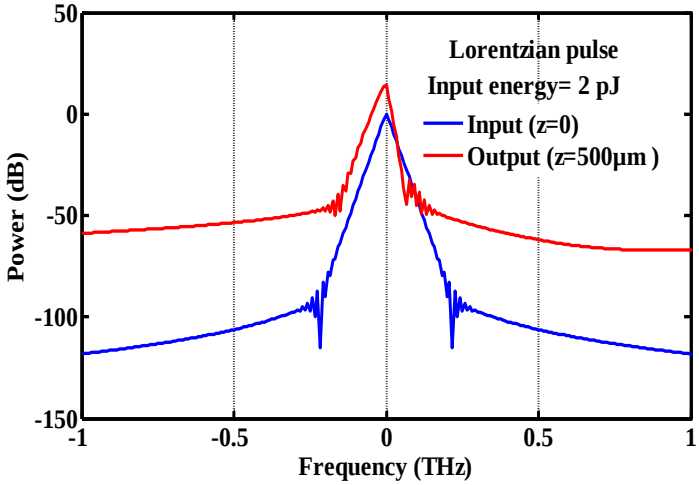

(c)

Figure 3.2: Frequency spectra of input and output pulse shapes for (a) Secant hyperbolic, (b) Gaussian, and (c) Lorentzian pulses.

Figure 3.2 shows the frequency spectra of input and propagated output pulses, which were obtained by performing the FFT on the temporal pulse shapes as shown in Figure 3.1. The amount of frequency shift is ~ -8.3 GHz for Secant hyperbolic and Gaussian pulses when the input pulse energy is 2 pJ. This means that the leading edge has a larger gain than the trailing edge that is due to the gain saturation of the SOA and SPM effects.

From Figure 3.2, it can be observed that the output spectral shape shifting depends on the input pulse energy. However, for weak input pulse energies (≤10 fJ), none of the output frequency spectra has been shifted toward lower frequencies. Note that there is no red-shifting occurring for the Lorentzian pulse when the input pulse energy is 2 pJ and the pulsewidth of 10 ps. That means more input pulse energy is required for occurring red shifting in Lorentzian pulse. A wider spectral broadening is observed for Gaussian pulse compared to the other two pulse shapes. Besides that, some oscillatory structures (i.e., dips) are observed in the higher frequency side of the frequency spectra, which is due to the SPM effects [8-9]. The physical mechanism behind the spectral shift and distortion is the SPM, occurring as a result of index non-linearities induced by the gain saturation [12, 35].

3.3.2 Pulse propagation characteristics for different input pulse shapes depending on CH relaxation time

In this sub-section, the pulse propagation characteristics for different input pulse shapes depending on the variation of CH relaxation time are discussed. When an optical signal is injected into the input facet of the SOA and SOA is biased with a direct current, a number of non-linear effects take place, each of those effects related to a specific transient time constant. There are two types of non-linear processes in SOA such as interband processes and intraband processes. When recombination of carriers between conduction and valence bands occurs, interband processes take place and intraband processes that take place without influencing the carrier density. When an optical pulse injects to the semiconductor active region, it is amplified due to stimulated emission what leads to carrier depletion. A few hundred of picoseconds of time constant are required by the carriers to return to their previous state. This recovery is expressed by carrier density pulsation.

Stimulated recombination burns a hole in the carrier distribution making it to deviate from the Fermi distribution. The time that carriers take to recover to the original Fermi distribution is of the order of tens of femtoseconds. This recovery process is commonly known as SHB. That means the carrier non-equilibrium is mainly governed by SHB effect and the distribution recovers to the equilibrium state by the carrier-carrier scattering process.

Carrier-carrier scattering also occurs due to TPA which influence the SOA response. A strong ultrafast pulse can generate free carriers by the TPA. These generated carriers reach to higher temperature than the lattice temperature and cool-down in a sub-picosecond time scale. Besides that, free carriers at low energy levels are removed due to stimulated emission or exited to higher energy levels due to free-carrier absorption (FCA). In this process the carrier temperature is increased and cools-down to the lattice temperature in a time scale of hundreds of femtoseconds. This process is expressed as CH [4, 17, 36].

In this section pulse propagation characteristics are investigated for different input pulse shapes depending on CH relaxation time. From the waveforms, it is observed that, output power decreases with the increase of CH relaxation time. It is also observed from the spectra that, the red shifting is not CH relaxation time dependent.

Figure 3.3 shows the waveforms and spectra for Secant hyperbolic pulse when (a) τ_{ch} = 400 fs, (b) τ_{ch} = 700 fs and (c) τ_{ch} = 1000 fs. The input pulse energy = 2 pJ and input pulsewidth is 10 ps. From the waveform it is observed that output power decreases with the increase of CH relaxation time. The output power is calculated 4.3 W, 4.2693 W and 4.2416 W for CH relaxation time 400 fs, 700 fs and 1000 fs respectively for Secant hyperbolic pulse. From the spectra it can be also observed that the amount of red shifting is unchanged with the change of CH relaxation time. The amount of red shifting remains same (~ -8.3 GHz) for all considered τ_{ch}.

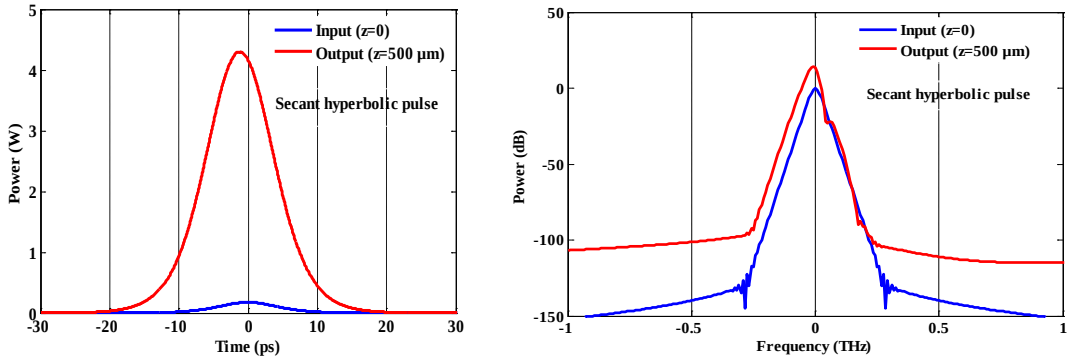

(a) τ_{ch} = 400 fs

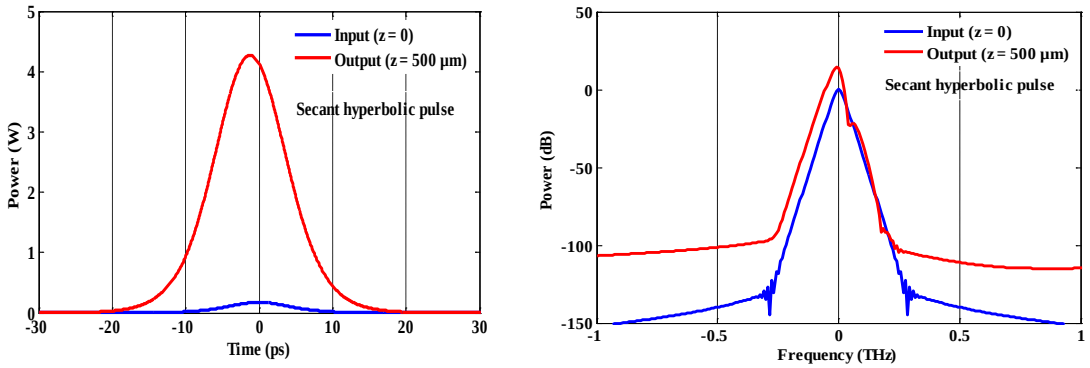

(b) τ_{ch} = 700 fs

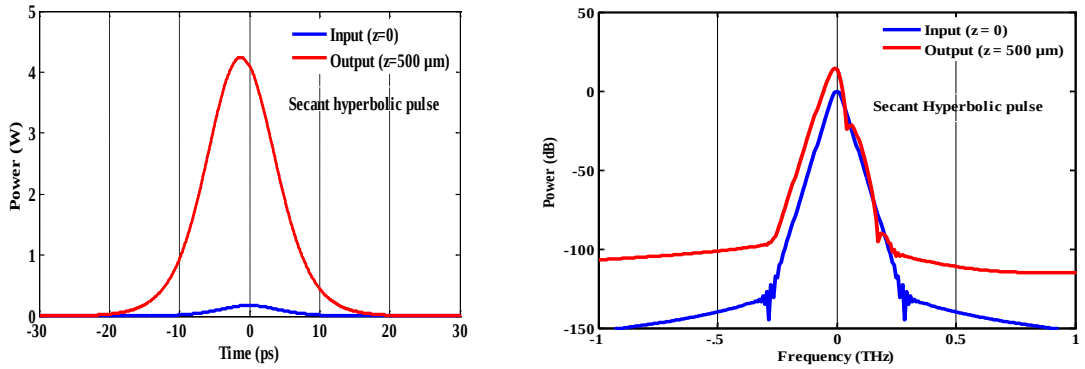

(c) τ_{ch} = 1000 fs

Figure 3.3: Waveform and spectra for Secant hyperbolic pulse when (a) τ_{ch} = 400 fs, (b) τ_{ch} = 700 fs and (c) τ_{ch} = 1000 fs.

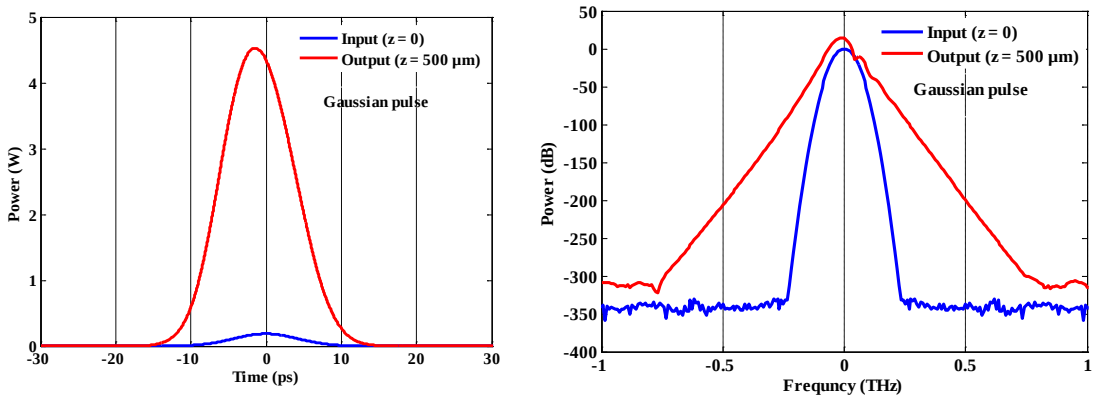

(a) τ_{ch} = 400 fs

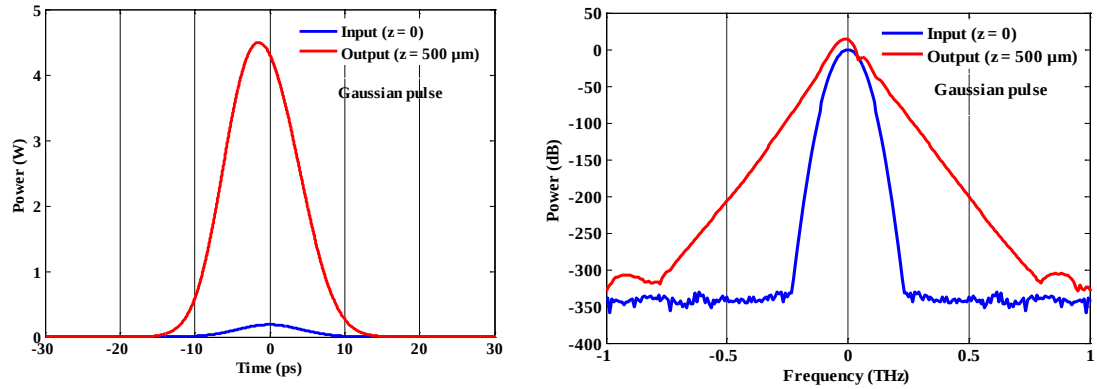

(b) τ_{ch} = 700 fs

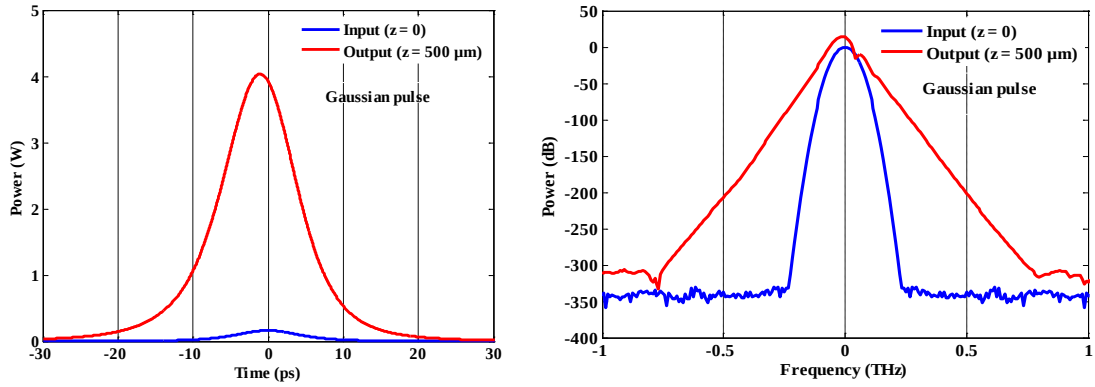

(c) τ_{ch} = 1000 fs

Figure 3.4: Waveforms and spectra for Gaussian pulse when (a) τ_{ch} = 400 fs, (b) τ_{ch} = 700 fs and (c) τ_{ch} = 1000 fs.

Figure 3.4 shows the waveforms and spectra for Gaussian pulse when (a) τ_{ch} = 400 fs, (b) τ_{ch} = 700 fs and (c) τ_{ch} = 1000 fs. From the waveforms, it is observed that output power decreases with the increase of CH relaxation time. The output power is

calculated 4.562 W, 4.526 W and 4.495 W for CH relaxation time 400 fs, 700 fs and 1000 fs respectively for Gaussian pulse. From the spectra it can be also observed that the amount of red shifting is unchanged with the change of CH relaxation time. The amount of red shifting remains same (~ -8.3 GHz) for all considered τ_{ch} as like as Secant hyperbolic pulse.

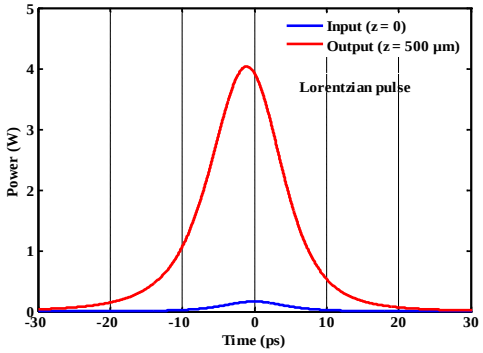

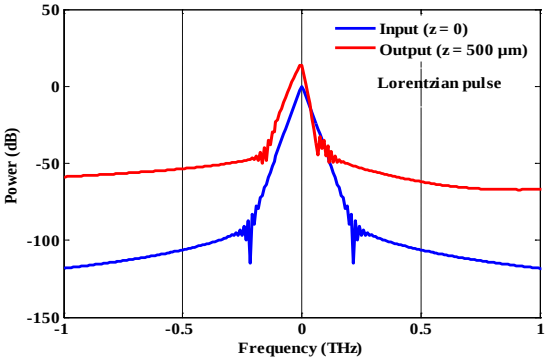

(a) τ_{ch} = 400 fs

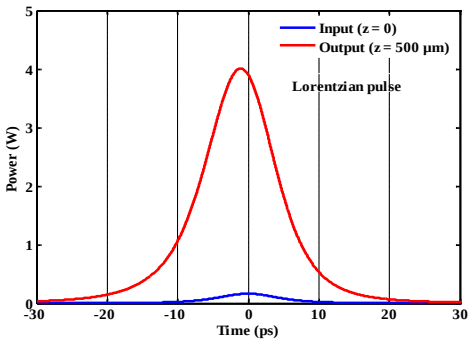

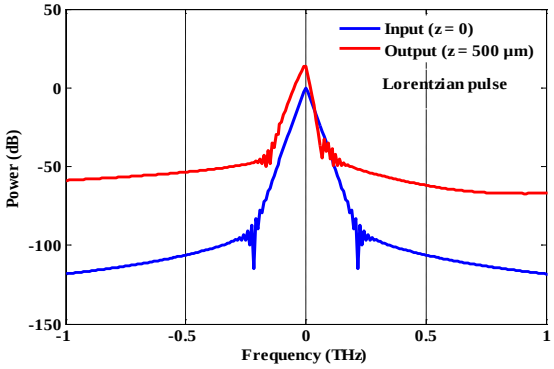

(b) τ_{ch} = 700 fs

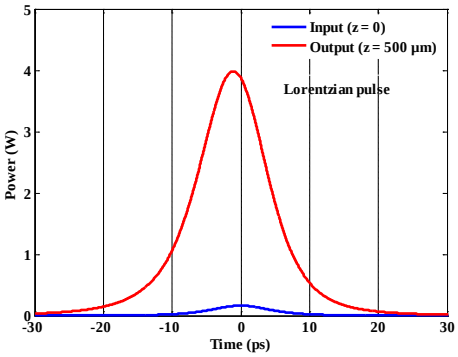

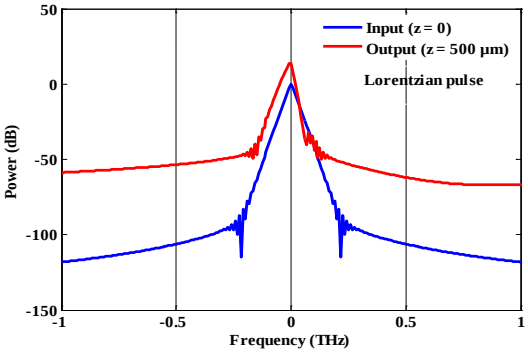

(c) τ_{ch} = 1000 fs

Figure 3.5: Waveform and spectra for Lorentzian pulse when (a) τ_{ch} = 400 fs, (b) τ_{ch} = 700 fs and (c) τ_{ch} = 1000 fs.

Figure 3.5 shows the waveform and spectra for Lorentzian pulse when (a) τ_{ch} = 400 fs, (b) τ_{ch} = 700 fs and (c) τ_{ch} = 1000 fs. From the waveform it is observed that output power decreases with the increase of CH relaxation time. The output power is calculated 4.035 W, 4.009 W and 3.985 W for CH relaxation time 400 fs, 700 fs and 1000 fs respectively for Lorentzian pulse. From the spectra it can be also observed that there is occurring no red shifting for Lorentzian pulse.

Comparing figures 3.3, 3.4 and 3.5, it can be said that, output power decreases with the increase of CH relaxation time for all those three input pulse shapes. From the waveform, sharpening of the leading edge is observed which is a common feature of all amplifiers. From the output spectra, multi peak structure can be observed for all considered input pulse shapes but the dominant peaks shift toward longer wavelength (red shift). This red shifting is occurred for Secant hyperbolic pulse and Gaussian pulse but not for Lorentzian pulse. This result is also found in above section when propagation characteristics was analyzed and compared for these three pulse shapes depending on input energy. That means red shifting in output spectra is not CH relaxation time dependent. Some oscillatory structures (i.e., dips) are observed in the higher frequency side of the frequency spectra for all pulse shapes, which is due to the SPM effects [8-9].

3.4 Conclusion

In this chapter, optical pulse propagation characteristics in SOA have been analyzed and compared for different input pulse shapes depending on different input energy levels and CH relaxation time. It has been observed from the output waveforms that, the peak positions are shifted toward the leading edge due to the gain saturation of the SOA. Higher output pulse energy was obtained by Gaussian pulse shape. Several dips are observed in the higher frequency side of the output spectra due to the SPM effect. For Secant hyperbolic and Gaussian pulses, the output spectra are red-shifted when the input energy ~2 pJ but Lorentzian pulse is not red-shifted.

It was also found that, output power increases with the decrease of CH relaxation time. For a particular CH relaxation time, higher output power is achieved by Gaussian pulse and lower output power is achieved by Lorentzian pulse. Moreover, the calculated red shifting is ~ -8.3 GHz for Secant hyperbolic and Gaussian pulse and it remains unchanged with the change of CH relaxation time. There is occurring no red shifting for Lorentzian pulse with the change of CH relaxation time.

From the above discussions, it can be said that, red shifting is input pulse energy dependent but it does not depend on the CH relaxation time.

Chapter 4
Gain Saturation Characteristics in SOA

This chapter discussed the gain saturation characteristics for different input pulse shapes in SOA depending on input FWHM and CH relaxation time. Here the results of gain saturation characteristics for different input pulse shapes are analyzed and compared.

4.1 Introduction

SOA has become a key component in high-speed communication system because of its high gain over a wide bandwidth. Therefore, it is important to study how the gain saturation may affect the SOA's performance. Several researches have been done to study the saturation behaviour of SOA using optical pulse [8, 33-34, 37]. The early studies showed that, for the injected pulse with pulse duration much less than the carrier lifetime, the gain is dependent on pulse energy but not on pulsewidth [8, 33-34]. Later, the saturation behaviour was studied for InGaAsP optical amplifier for input pulsewidth 15 ps and 150 fs and the measured saturation output energies were 150 fJ and 40 fJ respectively [38]. This input pulsewidth dependence of the gain saturation also agrees with the theoretical and experimental results for 1.5 μm SOA [39-40].

For lower input pulse energy, the gain remains unsaturated (linear gain). The gain reaches to the saturation when the input pulse energy is increased above a certain level and gives a non-linear response to the output power. For short input pulsewidth, the gain saturates at small output energy. This is due to the intraband dynamics such

as SHB and CH which are recognized as the main intraband processes that lead to gain saturation. For this reason, gain saturation characteristics have been investigated depending on different input parameters. In this section, gain saturation characteristics are analyzed and compared for different input pulse shapes depending on input FWHM and CH relaxation time.

The following equation has been used for calculating the gain in dB,

$$G = 10\log 10\left(E_{out} / E_{in}\right) \tag{4.1}$$

where

G = gain

E_{in} = input pulse energy

E_{out} = output pulse energy

4.2 Simulation Results and Discussions

4.2.1 Gain Saturation Characteristics for different input pulse shapes depending on input FWHM

Figure 4.1 shows the saturated gain versus output pulse energy characteristics for input pulse shapes: (a) Secant hyperbolic, (b) Gaussian, and (c) Lorentzian. These pulses are Fourier transform limited. The FWHM of the input pulses are 0.5 ~ 10 ps. The saturation behavior is different for short (<1 ps) and long (>1 ps) pulses. With the low input pulse energies (such as, ~0.1 pJ), the gain is unsaturated (i.e., a linear gain). Also, when the input pulse duration is short (<1 ps) then the gain saturates at low output energies. That is true for all the three input pulse shapes. It can be observed clearly that the gain saturation is pulsewidth dependent and output saturation energy increases with the increase of pulsewidth [12, 35, 38]. Comparing among three pulse shapes, it is clearly observed that gain saturates at higher output energy for Lorentzian input pulse shape with particular input pulse energy and achieve higher gain for all pulsewidths.

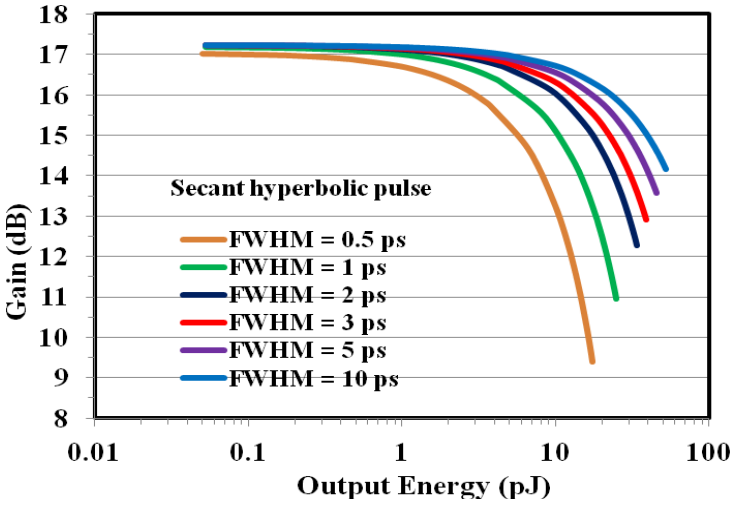

(a)

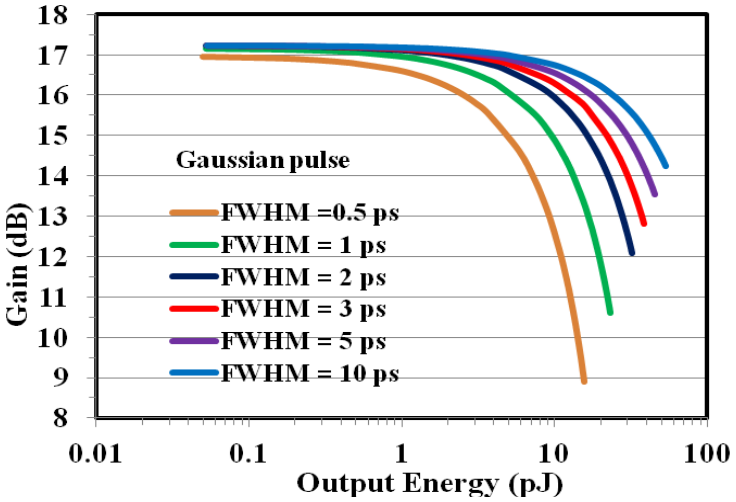

(b)

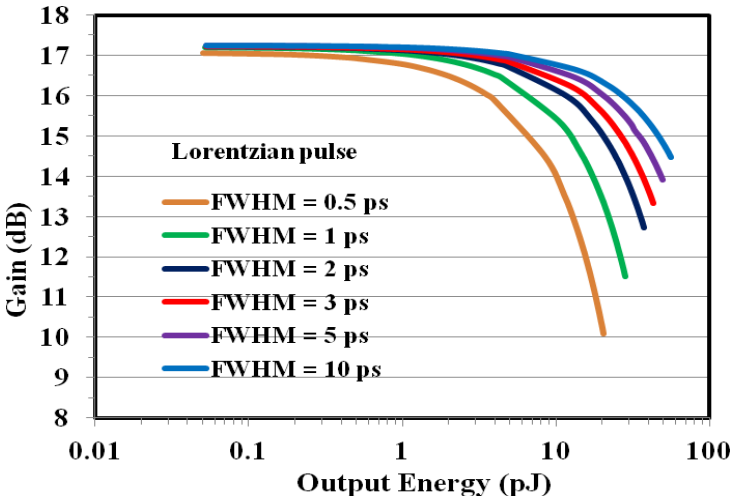

(c)

Figure 4.1: Gain saturation characteristics for different types of input pulses with different FWHM, such as 0.5-ps to 10-ps. The pulses are: (a) Secant hyperbolic, (b) Gaussian and (c) Lorentzian.

4.2.2 Comparison of Gain Saturation Characteristics in SOAs depending on input FWHM

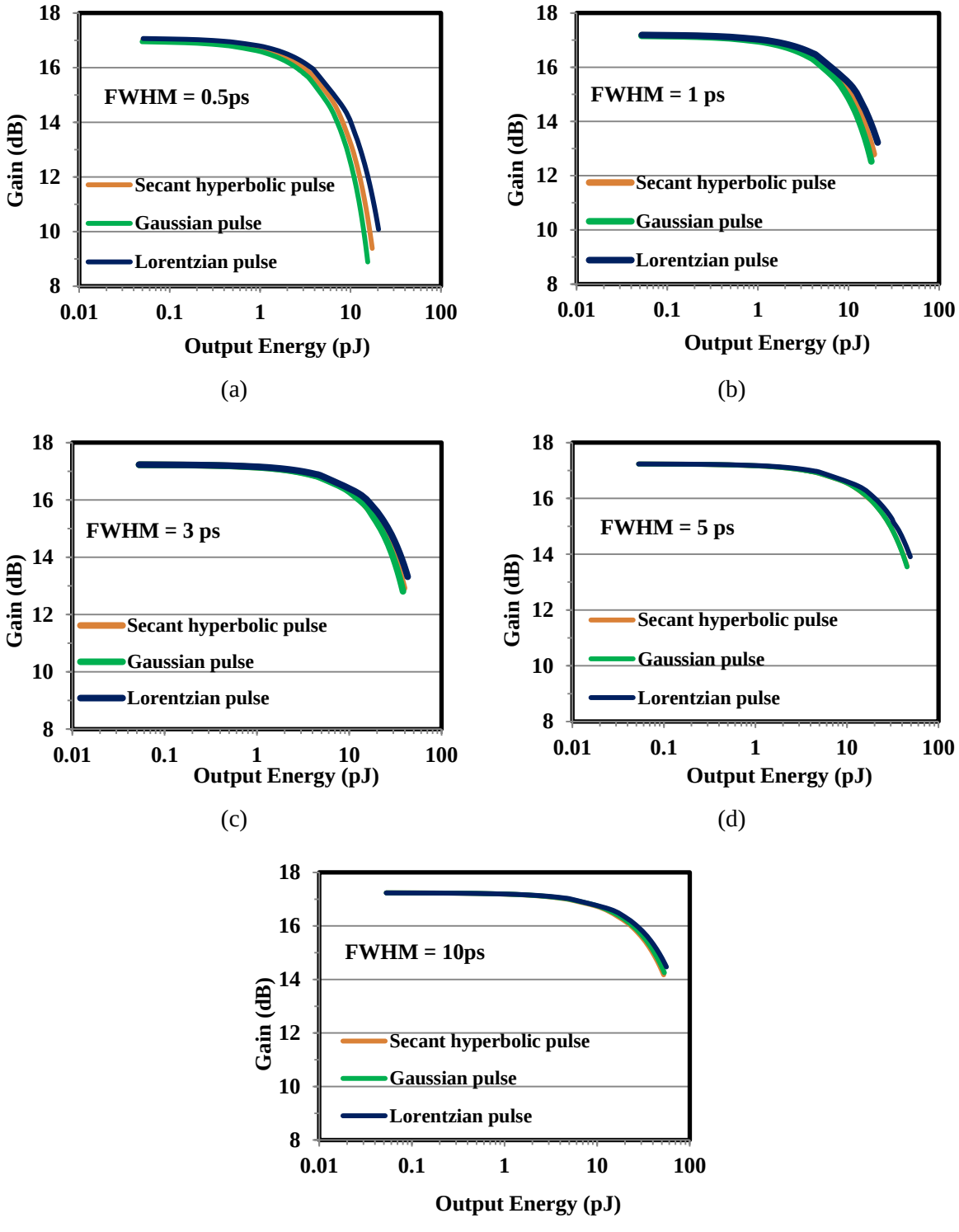

Figure 4.2: Gain saturation characteristics for different input pulse shapes, when (a) FWHM = 0.5 ps, (b) FWHM = 1 ps, (c) FWHM = 3 ps, (d) FWHM = 5 ps and (e) FWHM = 10 ps.

Figure 4.2 shows the comparison of gain saturation among the different input pulse shapes, when (a) FWHM = 0.5 ps (b) FWHM = 1 ps, (c) FWHM = 3 ps, (d) FWHM = 5 ps and (e) FWHM = 10 ps. When FWHM = 1 ps, the corresponding 3-dB down output saturation energies are found 14.08 pJ, 13.89 pJ and 14.42 pJ for Secant hyperbolic, Gaussian, and Lorentzian pulses, respectively. That means higher saturation output energy has been obtained for Lorentzian pulse shape and its true for all considered pulse duration (such as 0.5 ps- 10 ps).The linear gain is very similar for all the pulse shapes when the input pulse energy is low (such as, ~0.5 pJ). From the figures, it can be observed that, with the increase of pulse duration, the gain saturation characteristics are becoming similar for Secant hyperbolic and Gaussian pulse shapes. When FWHM = 0.5 ps, we can see three identical lines for three pulse shapes (not overlapped). However, with the increase of input FWHM (such as, 3 ps-10 ps), the gain saturation characteristics is becoming very similar (as overlapped) for Secant hyperbolic and Gaussian pulses. It is clear from the simulation results that for shorter pulse duration (~1 ps) all pulse shapes reaches saturation faster compared to longer pulse duration (>1 ps) scenario.

4.2.3 Gain Saturation Characteristics for different input pulse shapes with different CH relaxation time

Figure 4.3 shows the gain saturation characteristics for (a) Secant hyperbolic pulse, (b) Gaussian pulse and (c) Lorentzian pulse depending on CH relaxation time (such as 400 fs-1000 fs). From the figures, it can be observed that, for lower input energies (.001 pJ-.005 pJ) there is no change in output energies with the change of CH relaxation time. For a particular input energy the output energy decreases with the increase of CH and it is true for all pulse shapes. For example, the calculated output energies for Gaussian pulse are 53.497 pJ, 53.225 pJ and 52.964 pJ for CH relaxation time 400 fs, 700 fs and 1000 fs respectively when input energy 2 pJ. The calculated output energies for Secant hyperbolic pulse are 35.957 pJ, 35.894 pJ and 35.832 for CH relaxation time 400 fs, 700 fs and 1000 fs respectively when input energy 1 pJ.

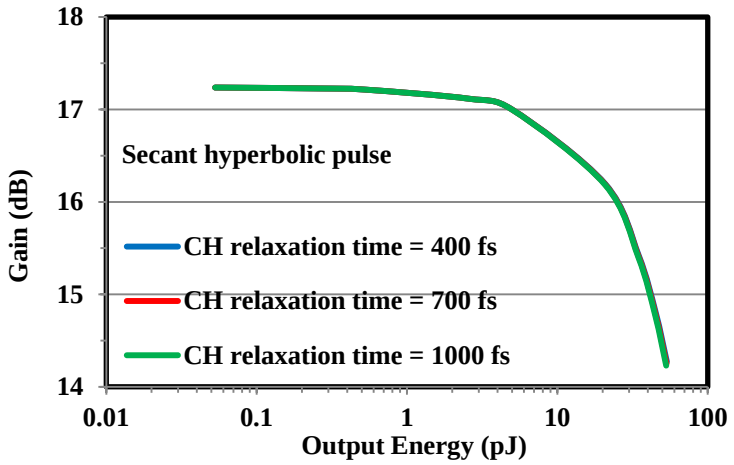

(a) Secant hyperbolic pulse

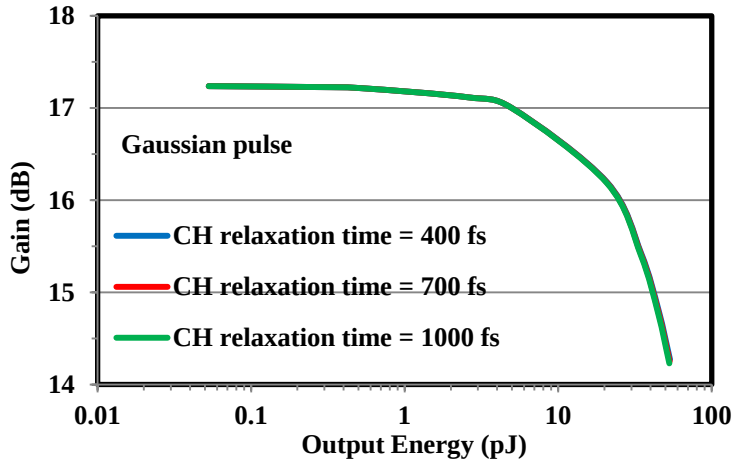

(b) Gaussian pulse

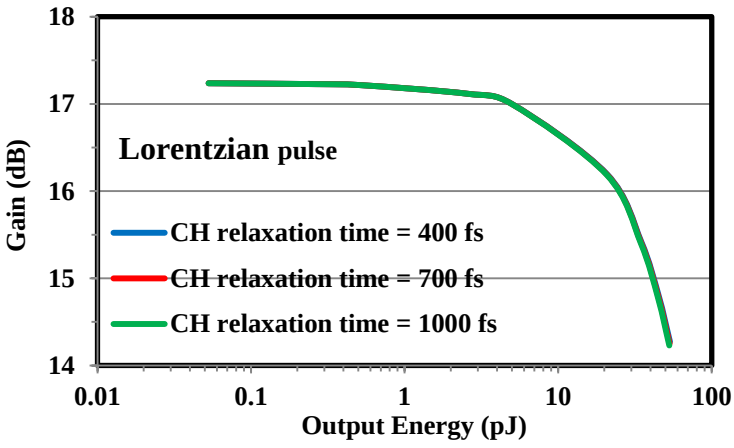

(c) Lorentzian pulse

Figure 4.3: Gain saturation characteristics for different types of input pulses with different CH relaxation time, such as 400 fs to 1000 fs. These are: (a) Secant hyperbolic pulse, (b) Gaussian pulse, and (c) Lorentzian pulse.

Higher output saturation energy is calculated for τ_{ch} = 400 fs and lower output saturation energy is found for τ_{ch} = 1000 fs in all three pulse shapes which means output saturation energy increases with the decrease of CH relaxation time and vice versa. For a particular CH relaxation time, higher output saturation energy is calculated for Gaussian pulse shape and lower output saturation energy is calculated for Secant hyperbolic pulse which means Secant hyperbolic pulse reaches to saturation faster than other two pulses.

4.3 Conclusion

Gain saturation characteristics for different input pulse shapes has been investigated and compared in this chapter depending on different input parameters. When gain saturation characteristics are analyzed depending on input pulsewidth, it is observed that, higher output pulse energy was obtained by Lorentzian pulse shapes. The saturated output pulse energy increases with the increase of pulsewidth for all pulse shapes. Moreover, the gain saturation characteristics for Secant hyperbolic and Gaussian pulses are becoming very similar when the pulsewidth is >1 ps.

Besides that, output saturation energy increases with the decrease of CH relaxation time and vice versa. For a particular CH relaxation time, higher output saturation energy is calculated for Gaussian pulse shape and lower output saturation energy is calculated for Secant hyperbolic pulse. That means Secant hyperbolic pulse reaches to saturation faster compared to the Gaussian and Lorentzian pulses and it is true for all considered input pulsewidth and CH relaxation time.

Chapter 5
Autocorrelation traces of FWHM for different input pulse shapes

This chapter describes the autocorrelation traces of FWHM for different input pulse shapes. The normalized difference of FWHM has been analyzed for different input pulse shapes. It shows how the output FWHM broadened with the input FWHM. Pulse propagation characteristics for higher to lower input pulse energies have been also discussed and compared.

5.1 Introduction

Non-linear pulse propagation characteristics for different input optical pulse shapes with various input pulse energy levels in SOAs has been investigated in this chapter. For simulation of non-linear pulse propagation, FD-BPM is used to solve the MNLSE in this research. In the MNLSE, gain spectrum dynamics, gain saturation are taken into account which depends on CD, CH, SHB, GVD, SPM and TPA.

After pulse propagation through the active region of SOA, amplification occurred and the output pulsewidth widens. This happens due to spectral broadening induced by SPM. The amount of broadening is calculated depending on input energies for all considered input pulse shapes. We also analyzed and compared the normalized difference of FWHM for different input pulse shapes in the SOA. To achieve the results, autocorrelation trace is used to analyze the series of data with normalization in time domain. We have investigated how the output FWHM broadened in relation to the input FWHM and input pulse energies for different input pulse shapes.

Figure 5.1 shows the (a) input pulse and (b) output pulse with the calculated FWHM using autocorrelation. Here, the input energy is 2 pJ and input FWHM is 10 ps and

the input pulse shape is Secant hyperbolic. In the next section, the output FWHM is calculated for different input pulse shapes with different input pulse energy levels and different the input FWHM. For calculating the FWHM, input power (W) and output power (W) have been normalized in time domain. From the figure, it is clear that, the output FWHM increases after amplification and the amount of normalized difference of FWHM is 15.2%. In this chapter, it is shown that, how the output FWHM broadened with the change of input FWHM for different input pulse shapes. Moreover, the results have been compared.

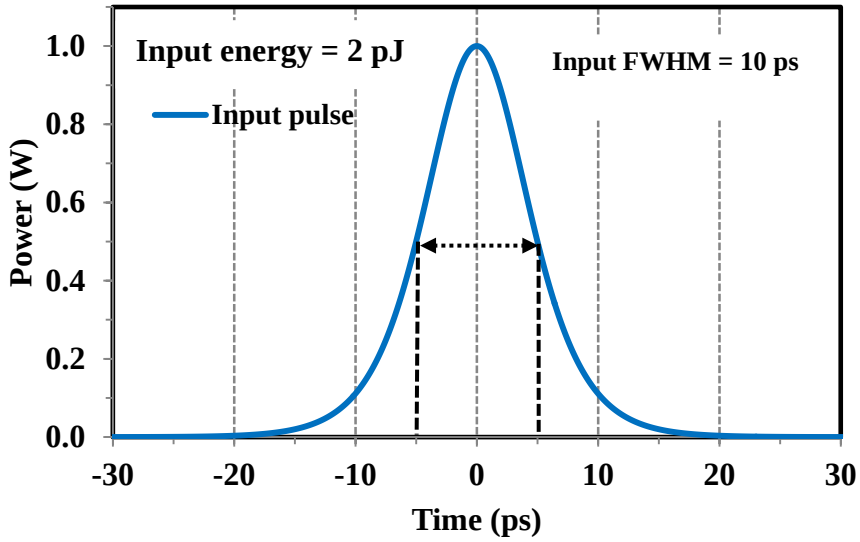

(a)

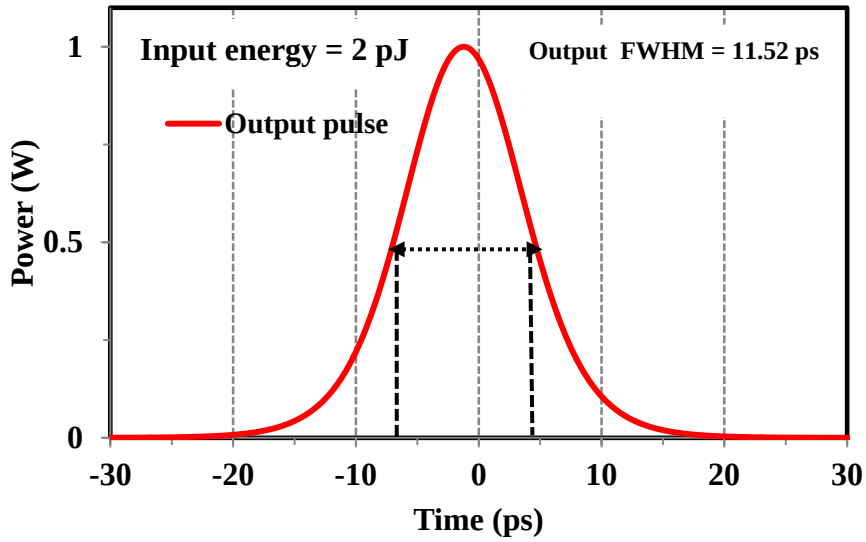

(b)

Figure 5.1: FWHM calculation for (a) input pulse and (b) output pulse

5.2 Simulation Results and Discussions

5.2.1 Pulse propagation depending on different input energies for different input pulse shapes

The simulation results of non-linear single optical pulse propagation characteristics in an SOA will be discussed for different energy levels in this section. The considered the input pulse width is 10 ps for different energy levels.

5.2.1.1 Output waveform for different input pulse shapes

The output waveforms for Secant hyperbolic pulse shape, Gaussian pulse shape and Lorentzian pulse shape are shown in Figure 5.2 when the input pulse energies are (a) 2 pJ, (b) 1 pJ and (c) 500 fJ, respectively. The sampling time step (Δt) is considered as 0.025 ps. It is clearly observed that higher output pulse energy is achieved by Gaussian pulse and lower output energy is achieved by Lorentzian pulse for all the level of input pulse energies (high to low). The calculated peak output powers are 4.2693 W, 4.5268 W, and 4.0091 W for Secant hyperbolic, Gaussian and Lorentzian pulses, respectively when input energy is 2 pJ. For the input energy 1 pJ, the calculated peak output powers are 2.89 W, 3.06 W and 2.71 W for Secant hyperbolic, Gaussian and Lorentzian pulses, respectively. However, when the input energy is low (i.e., 500 fJ), the calculated peak output powers are 1.77 W, 1.88 W, and 1.66 W for Secant hyperbolic, Gaussian and Lorentzian pulses, respectively. From these results, it can be confirmed that the higher output pulse energy can be achieved for higher input energy for all those three pulse shapes and vice versa. As the input pulse width is much shorter than the considered carrier lifetime, the leading edge of the pulse saturates the amplifier and the trailing edge experiences a lower gain, so the output pulse shape becomes asymmetric. Comparing all three pulse shapes with different input pulse energy levels, it can be observed that the output pulse shapes become more asymmetric for higher input energy and less asymmetric for the lower input energy levels.

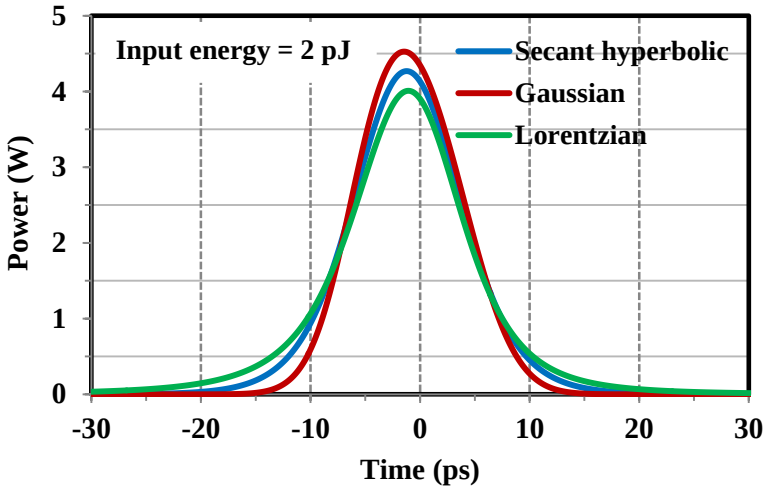

(a)

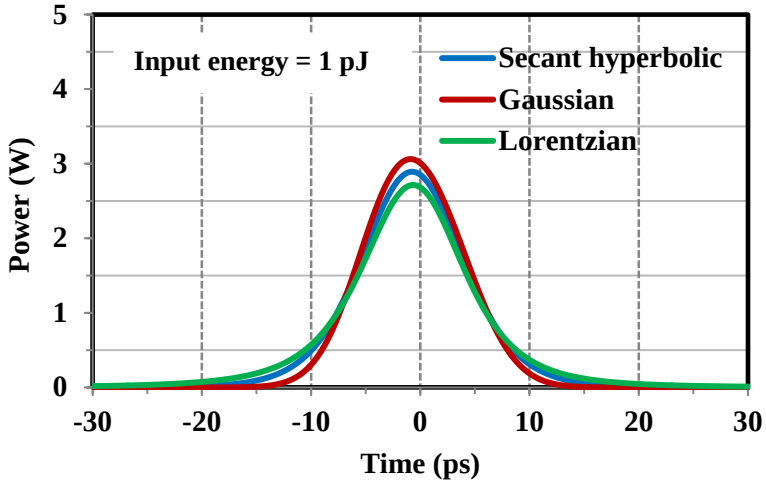

(b)

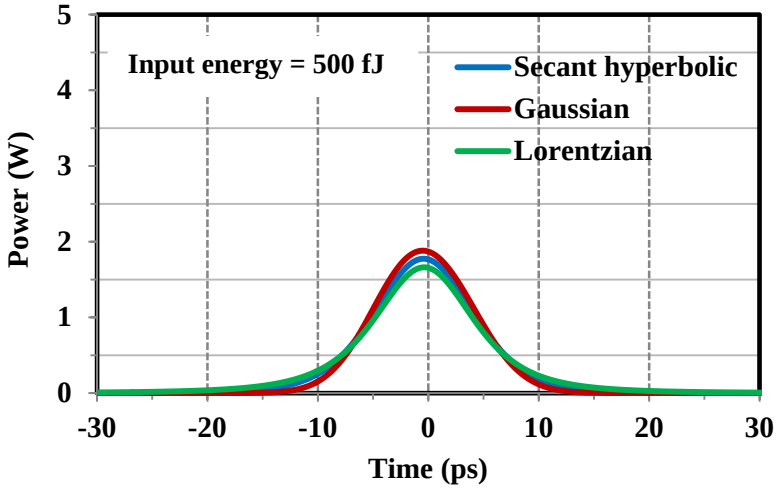

(c)

Figure 5.2: Output waveform for Secant hyperbolic pulse, Gaussian pulse and Lorentzian pulse when input energies are: (a) 2 pJ, (b) 1 pJ and (c) 500 fJ.

5.2.1.2 Output spectra for different input pulse shapes

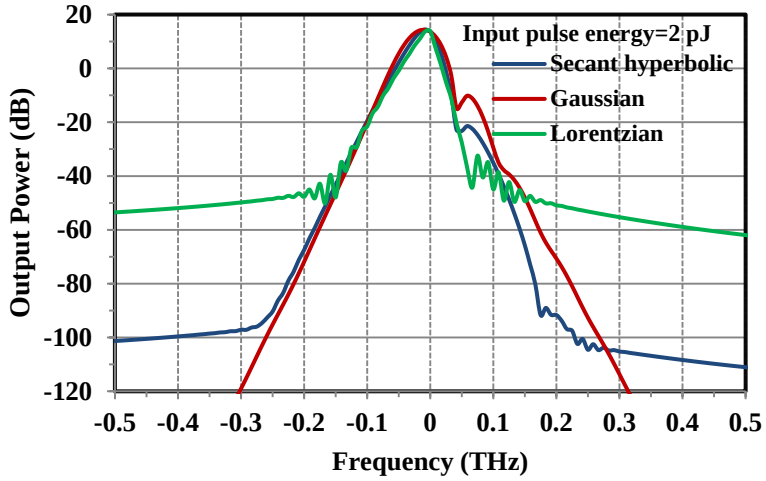

(a)

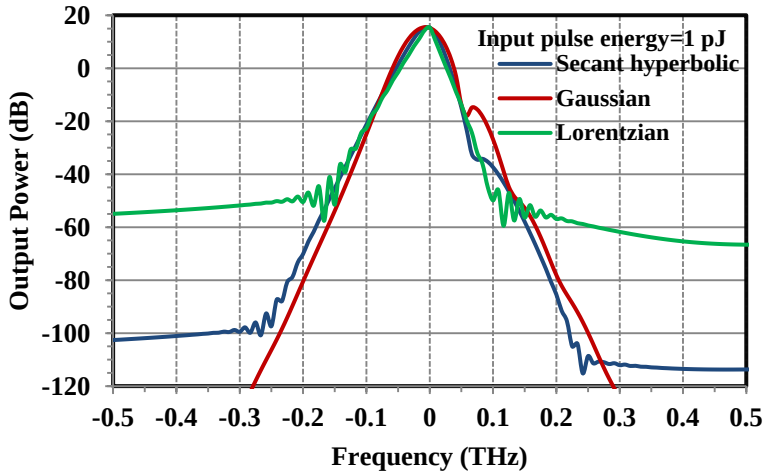

(b)

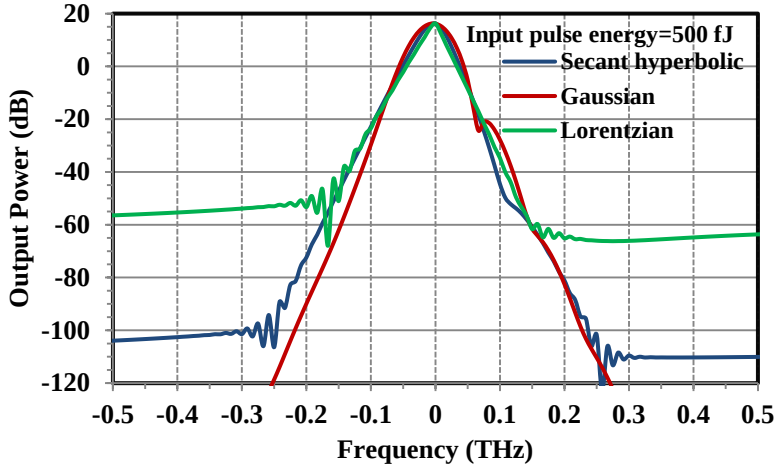

(c)

Figure 5.3: Output spectra for Secant hyperbolic pulse, Gaussian pulse and Lorentzian pulses when input energies are: (a) 2 pJ, (b) 1 pJ and (c) 500 fJ.

Figure 5.3 shows the frequency spectra of propagated output pulses for Secant hyperbolic pulse shape, Gaussian pulse shape and Lorentzian pulse shapes when the input pulse energies are: (a) 2 pJ, (b) 1 pJ and (c) 500 fJ. The frequency spectra were obtained by performing the FFT on the temporal pulse shapes as shown in Figure 5.2. The output spectral shape shifting is observed toward the lower frequency side, which is due to the gain saturation of the SOA and the SPM effects. For weak input pulse energies (i.e., ≤500 fJ), none of the output frequency spectra has been shifted toward the lower frequency side. It can be clearly seen from these figures that the output spectra is red-shifted and the amount of frequency shift is ~ -8.3 GHz for Secant hyperbolic and Gaussian pulses when the input pulse energy is 2 pJ and 1 pJ. While there is no red shifting is occurring for the Lorentzian pulse when the input pulse energy is 2pJ and 1 pJ. A wider spectral broadening is observed for Gaussian pulse compared to the other pulses, when the input energy is 2 pJ. Besides that some oscillatory structures (i.e., dips) are observed in the upper frequency side of the frequency spectra, which is due to the SPM effects [4-5]. The physical mechanism behind the spectral shift and distortion is the SPM, occurring as a result of index non-linearities induced by the gain saturation [4-5, 18]. From the simulated results, it has confirmed that there is no red shifting occurs in Lorentzian pulses for the considered pulse energies (i.e., 500 fJ ~ 2 pJ).

5.2.2 Output FWHM characteristics depending on different input energy levels

Figure 5.4 shows the characteristics of Output FWHM of (a) Secant hyperbolic pulse, (b) Gaussian pulse and (c) Lorentzian pulse for different input energies. After amplification the output FWHM always increases comparing to input FWHM except lower input energy such as 10 fJ. It happens because of spectral broadening induced by SPM. From the figures, it has been observed that, the output FWHM decreases with the decrease of input pulse energy. For particular input energy, when the input FWHM increases the output FWHM also increases. From this observation it can be said that, with the increase of input energy and input FWHM, the spectral shape broadens. For all input pulse energy, Lorentzian pulse achieved the wider output FWHM which means the output spectral shape broadening is larger than other two pulses. We also observed that, Gaussian pulse achieved shorter output FWHM

among all three pulse shapes. From the figures, it can be observed that for low input pulse energy (such as, 10-100 fJ), the output FWHM are almost similar (as overlapped) for all three input pulse shapes.

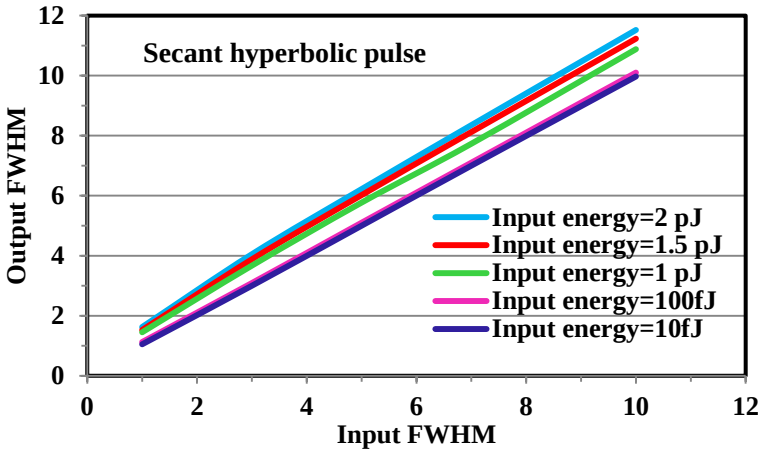

(a)

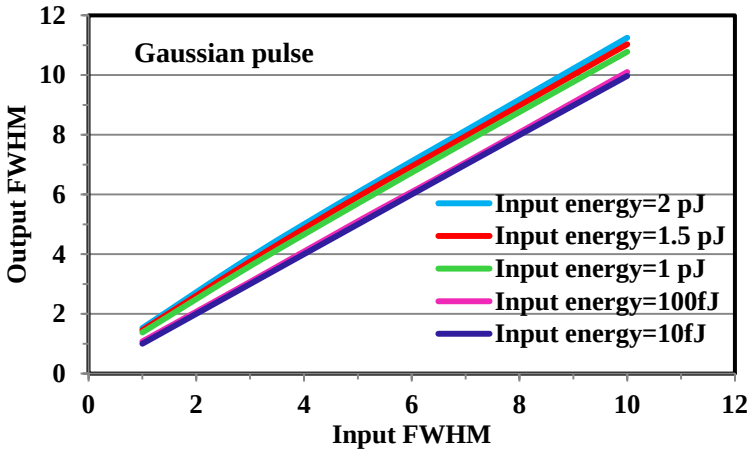

(b)

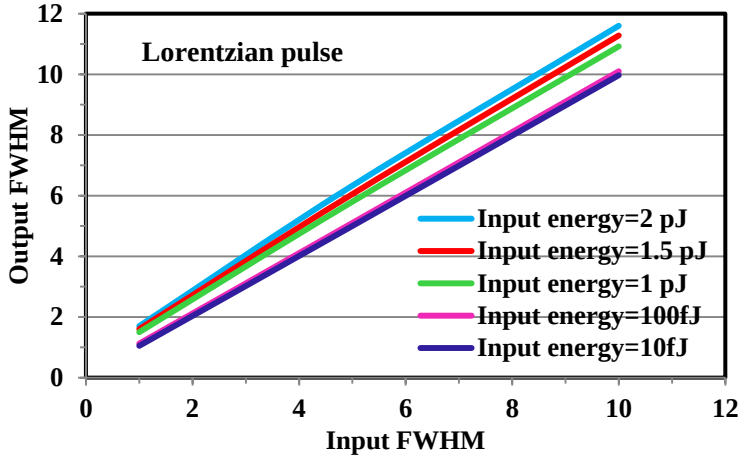

(c)

Figure 5.4: Characteristics of Output FWHM of (a) Secant hyperbolic pulse, (b) Gaussian pulse and (c) Lorentzian pulse for different input energy levels.

5.2.3 Normalized difference of FWHM

Figure 5.5 shows the normalized difference of FWHM versus input FWHM for different input pulse energies for (a) Secant hyperbolic pulse, (b) Gaussian pulse and (c) Lorentzian pulse. To achieve the results, autocorrelation trace is used to analyze the series of data with normalization waveforms. We have investigated how the output FWHM varies with the input FWHM and input pulse energies for different input pulse shapes. For particular input pulse energy, a higher percentage of increased output FWHM can be found for lower input FWHM and vice versa. For example, when the input pulse energy is 2 pJ, the output FWHM increases by 15.2%, 19.29%, 24.4%, 35% and 62.5% for the input FWHM of 10 ps, 7 ps, 5 ps, 3 ps and 1 ps, for the Secant hyperbolic pulse.

The similar results have been obtained for all three considered pulse shapes in this case study. It has been also observed that with the decrease of input pulse energy the percentage of increased output FWHM decreases for all input FWHM. From above observation, it can be concluded that, for a higher input energy with lower in put FWHM, the variation of output FWHM is the highest and lowest variation in output FWHM can be found for lower input energy with higher FWHM. Similar results have been calculated for all those three input pulses. But highest percentage of the difference of output FWHM has been calculated for Lorentzian pulse for all considered input energy along with input FWHM. For example, the calculated percentages are 16%, 15.2% and 12.5% for Lorentzian pulse, Secant hyperbolic and Gaussian pulse respectively, when input pulse energy is 2 pJ and the input FWHM is 10 ps.

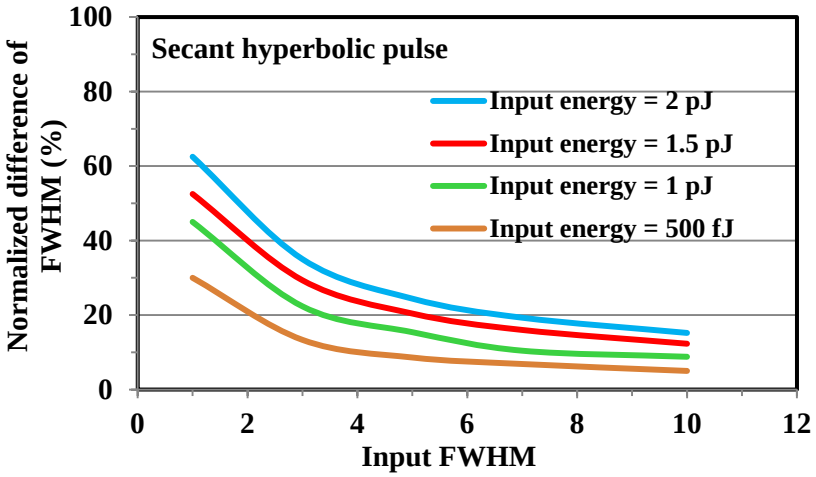

(a)

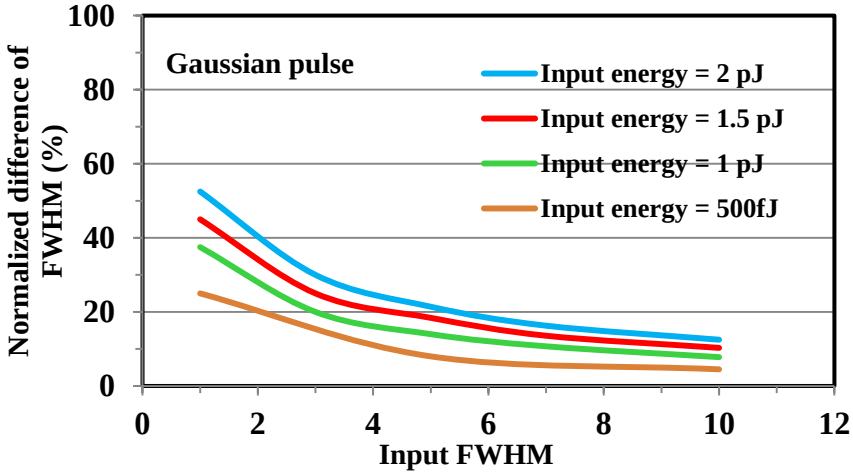

(b)

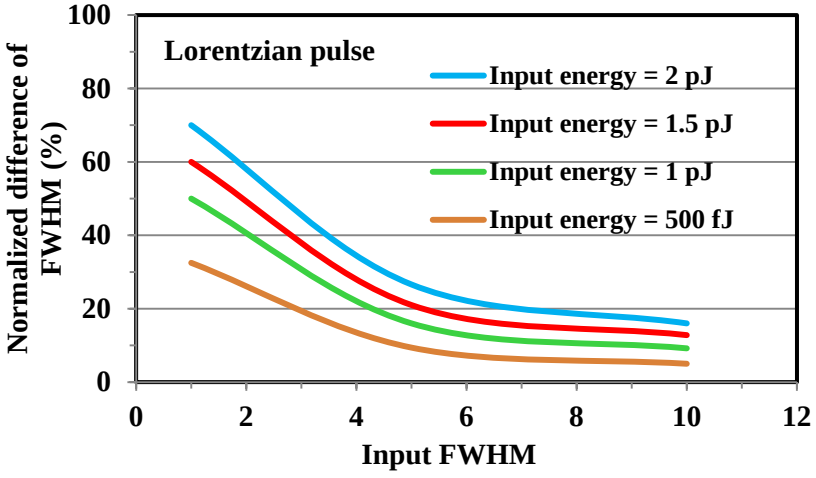

(c)

Figure 5.5: Normalized difference of FWHM versus input FWHM for different input pulse energy levels for (a) Secant hyperbolic, (b) Gaussian and (c) Lorentzian pulses.

5.3 Conclusion

In this chapter, non-linear optical pulse propagation characteristics have been analyzed with different input pulse shapes and different input pulse energy levels in SOAs for the autocorrelation traces of output FWHM. The higher output pulse energy is achieved for Gaussian pulse shape and the lower output pulse energy is achieved for Lorentzian pulse shape for all the considered input pulse energy levels. From the output frequency spectra, it has been clearly observed that red shifting does not occur for Lorentzian pulse for the considered input pulse energies (i.e., 500 fJ ~ 2 pJ).

The difference between the output and input FWHM of pulses also has been calculated for different input pulse shapes with the increase of input FWHM. From the calculation, it is found that, with the increase of input energy and input FWHM, the spectral shape broadens. For all input pulse energy, Lorentzian pulse achieved the wider output FWHM which means the output spectral shape broadening is larger than other two pulses. We also observed that, Gaussian pulse achieved shorter output FWHM among all three pulse shapes. From the figures, it can be observed that for low input pulse energy (such as, 10-100 fJ), the output FWHM are almost similar (as overlapped) for all three input pulse shapes.

Moreover, the normalized difference of FWHM has been calculated after normalizing the output pulse power. From the simulated results, it can be concluded that the percentage of difference of FWHM increases with the decrease of input FWHM and decreases with the increase of input FWHM.

Chapter 6
Conclusion and Future Work Recommendations

6.1 Conclusion

All optical devices should operate at faster speed for achieving high-speed communication. With the pulse shaping, it is possible to increase transmission speed without reducing accuracy or increasing the bandwidth. As the nonlinearities of SOA produce crosstalk and power penalty problems in long distance optical communication system, it is essential to optimize structural parameters of SOA in order to reduce the power penalty and bit error rate problem which arises due to gain saturation.

Considering above circumstance, in this research, single pulse propagation characteristics and gain saturation characteristics have been investigated and compared in SOA depending on different input pulse shapes such as Secant hyperbolic, Gaussian and Lorentzian pulse for designing high speed communication devices.

Analyzing the output waveforms, it can be observed that, the peak positions of the output pulse are shifted toward the leading edge due to the gain saturation of the SOA. Higher output pulse energy was obtained by Gaussian pulse shape. Moreover, output power increases with the decrease of CH relaxation time. For a particular CH relaxation time, higher output power is achieved by Gaussian pulse and lower output power is achieved by Lorentzian pulse.

Several dips are observed in the higher frequency side of the output spectra due to the SPM effect. For Secant hyperbolic and Gaussian pulses, the output spectra are red-shifted when the input energy ~2 pJ but Lorentzian pulse is not red-shifted. The calculated red shifting is ~ -8.3 GHz for Secant hyperbolic and Gaussian pulse and it

remains unchanged with the change of CH relaxation time. From this discussion it can be said that, red shifting is dependent with input pulse energy but not dependent with CH relaxation time.

Additionally, in this research the gain saturation characteristics in SOA has been analyzed and compared for different input pulse shapes depending on different input parameters such as, pulse width and the CH relaxation time. From the investigation, it is said that, the saturated output pulse energy increases with the increase of pulsewidth for all considered pulse shapes. Moreover, the gain saturation characteristics for Secant hyperbolic and Gaussian pulses are becoming very similar when the pulsewidth is >1 ps.

Besides that, output saturation energy increases with the decrease of CH relaxation time and vice versa. For a particular CH relaxation time, higher output saturation energy is calculated for Gaussian pulse shape and lower output saturation energy is calculated for Secant hyperbolic pulse. That means Secant hyperbolic pulse reaches to saturation faster compared to the Gaussian and Lorentzian pulses and it is true for all considered input pulsewidth and CH relaxation time.

The autocorrelation traces for FWHM are also analyzed for different input pulse shapes. The difference between the output and input FWHM of pulses also has been calculated for different input pulse shapes with the increase of input FWHM. From the obtained results, it can be said that, with the increase of input energy and input FWHM, the spectral shape broadens. For all input pulse energy, Lorentzian pulse achieved the wider output FWHM which means the output spectral shape broadening is larger than other two pulses. We also observed that, Gaussian pulse achieved shorter output FWHM among all three pulse shapes and for low input pulse energy (such as, 10-100 fJ), the output FWHM are almost similar (as overlapped) for all three input pulse shapes. After normalizing the output pulse power, the normalized difference of FWHM has been calculated. From the simulated results, it is found that, the percentage of difference of FWHM increases with the decrease of input FWHM and decreases with the increase of input FWHM.

The results those are found from the analysis and investigation of pulse propagation characteristics, gain saturation characteristics and autocorrelation traces in this

research, will be useful for the high-speed communication optical communication devices and systems design.

6.2 Future Work Recommendation

In this thesis, non-linear pulse propagation characteristics, gain saturation characteristics and autocorrelation traces for the output FWHM have been performed for Secant hyperbolic, Gaussian and Lorentzian pulse shapes. Other pulse shapes such as Single-sided Exponential pulse, Double-sided Exponential pulse and Sinc-shaped pulse can be considered for future research.

The propagation characteristics and wave mixing characteristics such as FWM, optical demultiplexing (DEMUX), optical phase-conjugation and time-delayed FWM characteristics in SOAs also can be investigated for different types of input pulse shapes to achieve the high conversion efficiency for future high-speed communication system.

Multi-wave mixing propagation characteristics using (i) Homogeneous pulse (Secant hyperbolic-Secant hyperbolic, Gaussian-Gaussian, Lorentzian-Lorentzian) or (ii) Heterogeneous pulse (Secant hyperbolic-Gaussian, Gaussian-Lorentzian, Secant hyperbolic-Lorentzian etc.) can be analyzed. Ongoing researches are required for achieving optimized results in modelling of the SOA.

References

[1] A. A. Shalaby, “Characterisation and optimisation of the semiconductor optical amplifier for ultra-high speed performance”. Doctoral Dissertation, Northumbria University, Newcastle, UK, 2012.

[2] A. A. E. Aziz, W. P. Ng, Z. Ghassemlooy, M. H. Aly and M. F. Chiang, “Optimisation of the key SOA parameters for amplification and switching” in proc of the 9th Annual Postgraduate Symposium on the Convergence of Telecommunications, Networking & Broadcasting, PGNET, Liverpool, pp. 107-111, 2008.

[3] X Yang, Q Weng and W Hu, “High-Speed All-Optical Switches Based on Cascaded SOAs”, Selected Topics on Optical Amplifiers in Present Scenario, InTech, pp. 25-46, 2012.

[4] N. Das, H. Kawaguchi and K. Alameh “Impact of Pump-Probe Time Delay on the Four Wave Mixing Conversion Efficiency in Semiconductor Optical Amplifiers” Advances in Optical Amplifiers, Ed. Prof.Paul Urquhart, InTech, pp. 129-146, 2011.

[5] N. K. Das, M. Razaghi and S. R. Hosseini, “Four-wave mixing in semiconductor optical amplifiers for high speed communication”, 5th International conference on Computers and Devices for Communication (CODEC), pp. 1-4, 2012.

[6] Y. Chung and N. Dagli, “An assessment of finite difference beam propagation method,” IEEE J. Quantum Electron., vol. 26, pp. 1335–1339, 1990.

[7] S. D. Conte and C. D. Boor, Elementary Numerical Analysis: An Algorithmic Approach, Third Edition, McGraw-Hill Book Company Co., Singapore, 1981.

[8] N. K. Das, Y. Yamayoshi and H. Kawaguchi, “Analysis of basic four wave mixing characteristics in a semiconductor optical amplifier by the finite-difference beam propagation method”, IEEE Journal of Quantum Electronics, vol. 36, no. 10, pp. 1184–1192, 2000.

[9] N. K. Das and N. C. Karmakar, “Nonlinear propagation and wave mixing characteristics of pulses in Semiconductor optical amplifiers”, Microwave and Optical Tech. letters, vol. 50, no. 5, pp. 1223-1227, 2008.

[10] S. R. Hosseini, M. Razaghi and N. K. Das, “Analysis of ultrafast nonlinear phenomena’s influences on output optical pulses and four-wave mixing characteristics in semiconductor optical amplifiers”, Opt. Quantum Electron, vol. 42(11–13), pp. 729–737, 2011.

[11] S. R. Hosseini, M. Razaghi and N. K. Das, “Analysis of non-linear refractive index influences on four-wave mixing conversion efficiency in semiconductor optical amplifiers,” Opt. Laser Tech., vol. 44, pp. 528–533, 2012.

[12] G. P. Agrawal and N. A. Olsson, “Self-Phase Modulation and spectral broadening of optical pulses in semiconductor laser amplifier”, IEEE Journal of Quantum Electronics, vol. 25, No. 11, pp. 2297-2306, 1989.

[13] N. K. Das, Y. Yamayoshi, T. Kawazoe and H. Kawaguchi, “Analysis of optical DEMUX characteristics based on four-wave mixing in semiconductor optical amplifiers”, IEEE /OSA J. Lightwave Technol., vol. 19, pp. 237-246, 2001.

[14] J. Xu, X. Zhang, J. Dong, D. Liu and Dexiu Huang, “High-speed all-optical differentiator based on a semiconductor optical amplifier and an optical filter”, Optics Letters, vol. 32, pp. 1872-1874, 2007.

[15] M. Connelly, “Semiconductor optical amplifiers” Kluwer academic Publishers, Boston, 2002.

[16] Y. Said and H. Rezig “SOAs Nonlinearities and Their Applications for Next Generation of Optical Networks”, Advances in Optical Amplifiers, Ed. Prof.Paul Urquhart, InTech, pp. 27-52, 2011.

[17] A. M. Melo “Nonlinear Applications of Semiconductor Optical Amplifiers for All-Optical Networks”, Doctoral Dissertation, Technical University of Berlin, 2007.

[18] G. P. Agrawal, “Nonlinear Fiber Optics”, Academic Press, Calif., San Diego, 1989.

[19] A. Yariv, “Optical Electronics”, 4th Edition, Saunders College Publishing, San Diego, 1991.

[20] E.G. Sauter, “Nonlinear Optics”, John Wiley & Sons, Inc. New York, 1996.

[21] A. Dienes, J. P. Heritage, C. Jasti and M. Y. Hong, “Femtosecond optical pulse amplification in saturated media”, J. Opt. Soc. Am. B, vol. 13, pp. 725-734, 1996.

[22] M. Y. Hong, Y. H. Chang, A. Dienes, J. P. Heritage, P. J. Delfyett, Sol Dijaili and F. G. Patterson “Femtosecond Self- and Cross-Phase Modulation in Semiconductor Laser Amplifiers”, IEEE Journal of selected topics in Quantum Electronics, vol. 2, no. 3, pp. 523-539, 1996.

[23] M. Y. Hong, Y. H. Chang, A. Dienes, J. P. Heritage and P. J. Delfyett, “Sub-picosecond pulse amplification in semiconductor laser amplifiers: Theory and experiment”, IEEE Journal of Quantum Electronics, vol. 30, pp. 1122–1131, 1994.

[24] M. Razaghi, A. Ahmadi, and M. J. Connelly, “Comprehensive finite-difference time-dependent beam propagation model of counter propagating picosecond pulses in a semiconductor optical amplifier”, IEEE/OSA Journal of Lightwave Tech., vol. 27, no. 15, pp. 3162-3174, 2009.

[25] K. Seki, T. Kamiya and H. Yanai, “Effect of waveguiding properties on the axial mode competition in stripe-geometry semiconductor lasers”, IEEE J. Electron., vol. 17, pp. 706-713, 1981.

[26] J. Leuthold, M. Mayer, J. Eckner, G. Guekos, H. Melchior and Ch. Zellweger, “Material gain of bulk 1.55 μm InGaAsP/InP semiconductor optical amplifiers approximated by a polynomial model”, J. Appl. Phys., vol. 87, pp. 618-620, 2000.

[27] K. Okamoto, “Theory of Optical Waveguides”, Corona Publishing Co., 1992.

[28] E. O. Brigham, “The Fast Fourier Transform and Its Applications”, Prentice Hall, 1988.

[29] M. Razaghi, A. Ahmadi, M. J. Connelly and K. A. Madanifar, “Numerical modelling of sub-picosecond counter propagating pulses in semiconductor optical amplifiers”, 9th International Conference on Numerical Simulation of Optoelectronic Devices (NUSOD), pp. 59-60, 2009.

[30] S. Barua, N. Das, S. Nordholm and M. Razaghi “Analysis of Gain Saturation Characteristics in SOAs for Different Input Pulse Shapes” 14th International conference on Numerical Simulation of Optoelectronics devices (NUSOD 2014), pp. 77-78, 2014.

[31] M. J. Connelly, L. P. Barry, B. F. Kennedy, D. A. Reid, “Numerical analysis of picoseconds pulse propagation in a tensile-strained semiconductor optical amplifier with parameter extraction using frequency resolved optical gating”, Optical and quantum electronics, vol. 40, pp. 411-418, 2008.

[32] N. K. Das, T. Kawazoe, Y. Yamayoshi and H. Kawaguchi, “Analysis of optical phase conjugate characteristics of picosecond four-wave mixing signals in semiconductor optical amplifiers” IEEE J. Quantum Electron., vol. 37, pp. 55-62, 2001.

[33] P. B. Hansen, J. M. Wiesenfeld, G. Eisenstein, R. S. Tucker and G.Raybon, “Repetition-rate dependence of gain compression in In-GaAsP optical amplifiers using picosecond optical pulses,” IEEE J. Quantum Electron., vol. 25, pp. 2611-2620, 1989.

[34] T. Saitoh and T. Mukai, “Gain saturation characteristics of traveling-wave semiconductor laser amplifiers in short optical pulse amplification,” IEEE J. Quantum Electron., vol. 26, pp. 2086-2094, 1990.

[35] P. Borri, S. Scaffetti, J. Mørk, W. Langbein, J.M. Hvam, A. Mecozzi and F. Martelli, “Measurement and calculation of the critical pulsewidth for gain saturation in semiconductor optical amplifiers”, Optics communication, vol. 164, pp. 51-55, 1999.

[36] S. Diez, All-optical signal processing by gain-transparent semiconductor switches, Ph.D. Thesis, Technical University of Berlin, 2000.

[37] A. Mecozzi and J. Mørk, “Saturation induced by picosecond pulses in semiconductor optical amplifiers”, J. Opt. Soc. Am. B, vol. 14, no. 4, pp. 761-770, 1997.

[38] Y. Lai, K. L. Hall, E. P. Ippen and G. Eisenstein, “Short pulse gain saturation in InGaAsP diode laser amplifiers,” IEEE Photon. Technol.Lett. vol. 2, pp. 711-713, 1990.

[39] K. L. Hall, G. Lenz, A. M. Darwish and E. P. Ippen, “Subpicosecond gain and index dynamics in InGaAsP diode Lasers”, Opt. Comm., vol. 111, pp. 589-612, 1994.

[40] K. L. Hall, E. R. Thoen and E. P. Ippen, “Nonlinearities in Active Media”, Nonlinear Optics in Semiconductor II, Semiconductors and Semimetals, ch. 2, vol. 59, pp. 83-160, Ed. Dean Elsa Garmire, Academic Press, San Diego, 1998.

Every reasonable effort has been made to acknowledge the owners of copyright material. I would be pleased to hear from any copyright owner who has been omitted or incorrectly acknowledged.